INVESTIGATION OF THE EFFECT OF AGING UNDER STRESS ON THE SHAPE MEMORY PROPERTIES OF Ni-RICH NiTiHf HIGH TEMPERATURE SHAPE MEMORY ALLOY

NİKELCE ZENGİN NiTiHf YÜKSEK SICAKLIK ŞEKİL HAFIZALI ALAŞIMIN ŞEKİL BELLEĞİ ÖZELLİKLERİNE GERİLME ALTINDA YAŞLANDIRMA ETKİSİNİN ARAŞTIRILMASI

HALDUN HALİS

PROF. DR BENAT KOÇKAR

Supervisor

Submitted to Graduate School of Science and Engineering of Hacettepe University
as a Partial Fulfilment to the Requirements
for the Award of the Degree of Master of Sciences
in Mechanical Engineering.

2022

ABSTRACT

INVESTIGATION OF THE EFFECT OF AGING UNDER STRESS ON THE SHAPE MEMORY PROPERTIES OF Ni-RICH NiTiHf HIGH TEMPERATURE SHAPE MEMORY ALLOY

Haldun HALİS

Master of Science, Department of Mechanical Engineering
Supervisor: Prof. Dr Benat KOÇKAR
June 2022, 43 Pages

Shape memory alloys (SMAs) are extraordinary materials having very high shape or strain recovery capabilities via martensite-austenite phase transformation. The shape recovery capability of SMAs can be effectively exploited to generate work against applied load.

To utilize SMAs as thermally activated actuators for aerospace applications, high transformation temperatures (TTs) that are beyond 100°C, are desired. NiTi based SMAs exhibits promising properties in terms of high strength and longer functional fatigue life with stable actuation properties, however, they cannot be utilized for high temperature application due to their relatively lower TT. TTs higher than 100°C can be attained when NiTi SMAs are alloyed with Au, Pd, Pt, Zr or Hf. Hf is the utmost favourable alloying element to NiTi Alloys to raise the TTs over 100°C without decreasing the strength of the alloy.

As the TTs of NiTi alloys are increased via alloying with Hf they are able to be used at higher temperatures and ternary NiTiHf alloys are named as high temperature shape memory alloys (HTSMAs) in the literature. These alloys lose their strength so, resistance

against plastic deformation decreases. Thus, the stability of the shape memory properties such as transformation temperatures (TTs), actuation strain (ε_{act}) and thermal hysteresis (T_{hys}) are mitigated. The loss of shape memory properties with the thermal or thermo-mechanical cycles is called as Functional Fatigue (FF) in SMA literature. To increase the stability of the functional shape memory properties of HTSMAs deformation and age hardening methods can be applied. In this study, Ni-rich Ni(50.3at%)Ti(30at%)Hf(20at%) HTSMA was used since it can be a deformation as well as an age hardenable alloy.

As cast alloy was solutionized to homogenize the chemistry of the materials. Then, thermal and thermo-mechanical treatments were conducted after solutionizing heat treatment. Stress free aging, stress assisted aging and cold rolling with successive aging treatments were applied. Aging time and temperature parameters were applied as 1 hour and 550°C, respectively in all aging treatments. 5% thickness reduction was applied in cold rolling operation. TTs of all thermally and thermo-mechanically processed samples were measured under stress free condition and functional fatigue experiments (FFEs) were run under 200MPa via thermally cycling the samples between the predetermined upper and lower cycle temperatures (UCT and LCT) to determine the evolution of the shape memory properties with the applied processes. Then, all the results were compared by taking the solutionized sample as the base sample.

Experiment results showed that highest functional fatigue life was achieved in the sample, which was cold rolled (CR) with 5% thickness reduction and then successively stress aged at 550°C for 1 hour under 200MPa. Additionally, cold rolling with successive stress aging treatment managed to obtain very stable but relatively lower ε_{act} values in Ni-rich Ni(50.3at%)Ti(30at%)Hf(20at%) HTSMA.

Keywords: Shape Memory Alloy, High Temperature Shape Memory Alloy, Stress Assisted Aging

ÖZET

NİKELCE ZENGİN NiTiHf YÜKSEK SICAKLIK ŞEKİL HAFIZALI ALAŞIMIN ŞEKİL BELLEĞİ ÖZELLİKLERİNE GERİLME ALTINDA YAŞLANDIRMA ETKİSİNİN ARAŞTIRILMASI

Haldun HALİS

Yüksek Lisans, Makina Mühendisliği Bölümü
Tez Danışmanı: Prof. Dr Benat KOÇKAR
Haziran 2022, 43 Sayfa

Şekil hafızalı alaşımlar (ŞHA), martenzit-östenit faz dönüşümleri yoluyla çok yüksek şekil geri kazanımı özelliğine sahip sıra dışı malzemelerdir. Şekil hafızalı alaşımların şekil geri kazanımı özelliği, mekanik yüklere karşı iş üretmek için etkin bir şekilde kullanılabilir.

Şekil hafızalı alaşımları havacılık uygulamalarında termal olarak aktive edilmiş eyleyiciler olarak kullanmak için 100°C'nin üzerindeki dönüşüm sıcaklıkları tercih edilir. NiTi bazlı şekil hafızalı alaşımları, stabil davranış, yüksek mukavemet ve daha uzun fonksiyonel yorulma ömrü açısından umut verici özellikler sergilemektedirler, ancak nispeten düşük dönüşüm sıcaklıkları nedeniyle yüksek sıcaklık uygulamalarında kullanılamazlar. NiTi bazlı şekil hafızalı alaşımlar Au, Pd, Pt, Zr veya Hf elementleri ile alaşımlandığında 100°C'den daha yüksek dönüşüm sıcaklıkları elde edilebilir. Hf, NiTi alaşımının mukavemetini düşürmeden dönüşüm sıcaklıklarını 100°C'nin üzerine çıkarmak için üzerinde çalışılan en umut verici üçüncül bir alaşımlama elementidir.

NiTi alaşımlarının dönüşüm sıcaklıkları, Hf ile alaşımlanarak yükseltilebildiğinden daha yüksek sıcaklıklarda kullanılabilirler ve NiTiHf alaşımları literatürde Yüksek Sıcaklık

Şekil Hafızalı Alaşımı (YSŞHA) olarak adlandırılır. Bu alaşımlar mukavemetlerini kaybettiklerinde plastik deformasyona karşı dirençleri de azalır. Bu durumda, dönüşüm sıcaklıkları, çalıştırma gerilimi ve termal histerezis gibi şekil hafıza özelliklerinin kararlılığı da azalır. Termal veya termo-mekanik çevrimler ile şekil hafızası özelliklerinin yitirilmesi, literatürde Fonksiyonel Yorulma olarak adlandırılır Yüksek Sıcaklık Şekil Hafızalı Alaşımlarının şekil hafızası özelliklerinin iyileştirilebilmesi için sıcak veya soğuk şekillendirme veya yaşlandırma yöntemleri uygulanabilir.

Bu çalışmada, soğuk şekillendirme ve yaşlandırma ile mekanik ve şekil hafızası özellikleri iyileştirebilen bir alaşım olan ve Ni bakımından zengin Ni(50,3at%) Ti(30at%) Hf(20at%) HTSMA kullanılmıştır. İlk olarak, döküm halde tedarik edilmiş malzemenin iç yapısını homojenleştirmek için çözündürme ısıl işlemi (Solution Heat Treatment) uygulanmıştır. Daha sonra soğuk şekillendirme, gerilimsiz (stress-free) yaşlandırma ve gerilme altında (stress-assisted) yaşlandırma işlemleri yapılmıştır. Tüm yaşlandırma ısıl işlemlerinde yaşlandırma sıcaklık ve süre parametreleri sırasıyla 550°C ve 1 saat olarak uygulanmıştır. Soğuk haddeleme işleminde ise kesitte %5 kalınlık düşürülmesi uygulanmıştır. Numunelerin dönüşüm sıcaklıkları, tüm termal ve termo-mekanik işlemler yapıldıktan sonra yük uygulanmadan ölçülmüştür.

Son olarak, şekil hafızası özelliklerinin gelişimini belirlemek için numunelerin önceden belirlenmiş üst ve alt çevrim sıcaklıkları arasında termal olarak 200MPa sabit yük altında çalıştırılması yoluyla fonksiyonel yorulma deneyleri yapılmıştır. Sonuçlar ise, sadece çözündürme ısıl işlemi uygulanmış durum referans alınarak karşılaştırılmıştır.

Deney sonuçlarına göre, %5 kalınlık azaltılarak soğuk haddelenmiş ve ardından 200MPa sabit gerilme altında 1 saat boyunca 550°C'de yaşlandırılmış numunede en yüksek fonksiyonel yorulma ömrünün elde edildiğini görülmüştür. Ek olarak, soğuk haddeleme ve ardından gerilme yaşlandırma işlemi, çok kararlı ancak nispeten daha düşük eyleyici gerinim değerlerinin elde edilmesini neden olmuştur.

Anahtar Kelimeler: Şekil Hafızalı Alaşım, Yüksek Sıcaklık Şekil Hafızalı Alaşım, Gerilim Altında Yaşlandırma

ACKNOWLEDGEMENTS

I would like to thank my supervisor Prof. Dr. Benat KOÇKAR for her technical support and guidance throughout my research. I also thank to my dear wife and my family for the support they have provided to me.

This study was supported by Turkish Aerospace under Grant no. DKTM/2015/10 and Hacettepe University Scientific Research Projects Coordination Unit under Grant No. 19314, therefore, I would like to express my sincere gratitude to both of the grants.

Haldun HALİS
June 2022, Ankara

TABLE OF CONTENTS

TABLE OF FIGURES

LIST OF TABLES

SYMBOLS AND ABBREVIATIONS

Symbols

A_f	Austenite Finish Temperature
A_s	Austenite Start Temperature
Hf	Hafnium
M_f	Martensite Finish Temperature
M_s	Martensite Start Temperature
Ni	Nickel
Ti	Titanium
T_{hys}	Thermal Hysteresis
ε_{act}	Actuation Strain
ε_{aus}	Austenite Strain
ε_{mar}	Martensite Strain

Abbreviations

AIS	Accumulated Irrecoverable Strain
CRed	Cold Rolled
DSC	Differential Scanning Calorimetry
EDM	Electrical Discharge Machining
HTSMA	High Temperature Shape Memory Alloy
LCT	Lower Cycle Temperature
NC	Number of Cycles
NP	Nano-Precipitates
SAD	Selected Area Diffraction
SMA	Shape Memory Alloy
SME	Shape Memory Effect
TT	Transformation Temperature
TWSM	Two Way Shape Memory
UCT	Upper Cycle Temperature
WEDM	Wire EDM

1. INTRODUCTION

Shape memory materials are unique materials that have the ability to generate work or recover deformations against applied load through martensitic–austenitic phase transformations. Binary NiTi alloys are scientifically most popular alloys among SMAs since their shape memory properties are exceptional such as showing high actuation strain (ε_{act}) and actuation stress, though their TTs are below 100°C [1]. In order to utilize NiTi SMAs as actuators at high temperatures, additional alloying elements such as Hafnium, Platinum, Zirconium etc. are added to binary alloy, which increases the TTs to higher levels [2, 3].

TTs are SMA's one of the most important properties which directly determine the activation temperature range and the medium of the utilization. TTs are called as Martensite Finish (M_f), Martensite Start (M_s), Austenite Start (A_s) and Austenite Finish (A_f), in the literature. The evolution of TT and ε_{act} and accumulated irrecoverable strain (AIS) values dictates the cyclic and thermal stability properties of the alloys through the thermal and/or thermo-mechanical cyclic loadings of SMAs.

Cyclic and thermal stability have high importance when the SMAs are used as an actuator since actuator applications require high positional precision. In this study, the effect of aging under tensile stress on the cyclic stability of solutionized and 5% cold rolled (CRed) Ni-rich Ni(50.3at%)-Ti(30at%)-Hf(20at%) specimens was studied. It has been already proved that the dimensional and thermal stability of the alloy can be improved with cold working and the formation of nano-precipitates (NP) since the deformation induced dislocations and NP increase the strength of the alloy [4]. As the strength increases, the resistance of the alloy to plastic deformation during martensite-austenite phase transformation under applied stress increases as well. However, there is no study to reveal the effect of stress-oriented precipitates together with the induced dislocations via cold rolling on the cyclic stability of this Ni-rich NiTiHf alloy under tensile loading until now. To understand the effect of nano-precipitate formations with stress aging (SA) on the cyclic stability of solutionized and CRed Ni-rich NiTiHf alloys, FFEs were conducted on Ni(50.3at%)-Ti(30at%)-Hf(20at%) samples, which were solutionized, stress free aged, aged under tensile stress and CRed and subsequently aged under tensile stress. Functional

fatigue lifetimes (FFL), TTs, martensite (ε_{mar}) and austenite strain (ε_{aus}) magnitudes together with T_{hys} values were drawn from all FFEs. It should be noted that ε_{aus} corresponds to accumulated irrecoverable strain (AIS) with the thermal cycles. All the functional properties were then compared for especially optimizing the dimensional stability of the alloy with the applied thermal and/or thermo-mechanical treatments. It was found that stress aging which was applied after cold rolling process tremendously improved FFL of Ni(50.3at%)-Ti(30at%)-Hf(20at%) alloy. The actuation together with AIS values significantly decreased and the stability of the ε_{act} and T_{hys} was maintained with cold rolling and successive stress aging process.

2. THEORY AND LITERATURE

2.1. Shape Memory Effect

Shape memory alloys (SMAs) demonstrate two distinct phases, which are called as martensite and austenite. When the SMA is cooled to a temperature below Martensite Start (M_s) under stress-free condition they display twinned martensite structure. If the alloy is stressed with an external force twinned martensite transforms to detwinned martensite and the variants of the twinned martensite plates orient themselves through the most favourably oriented martensite variant with respect to the applied load. Thus, shape change can be observed.

SMA recovers this shape change when the phase of alloy is transformed into fully austenite by heating it above A_f temperature. This behaviour is called as *Shape Memory Effect (SME)*. Finally, SMA returns to its initial twinned martensite structure when cooled below M_f temperature. SME route is also defined with a schematic in Figure 2.1.

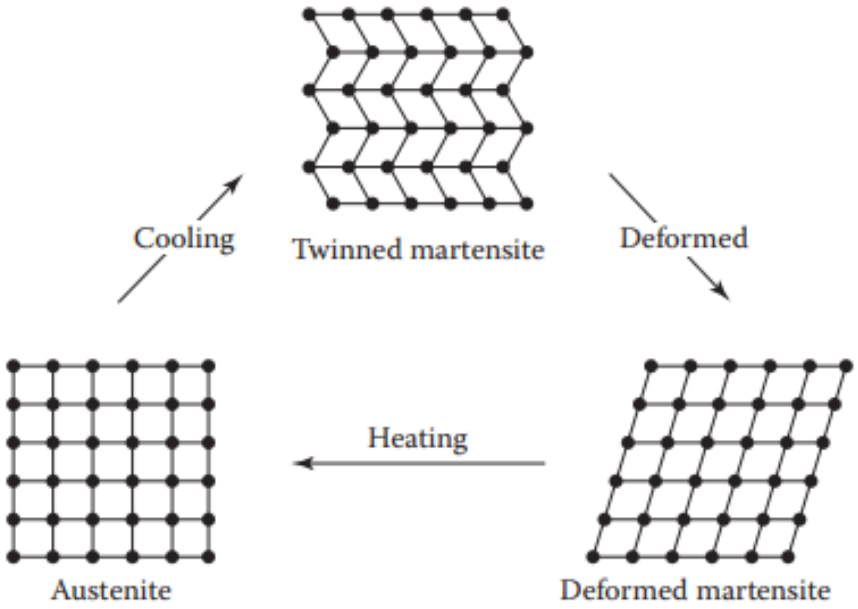

Figure 2.1. Schematic of SME [5].

2.2. Superelasticity Effect in SMAs

Superelasticity or in other words *Pseudoelasticity* phenomenon is defined as the transformation between austenite and martensite under the effect of stress at a constant temperature. While SMA is staying in its austenitic phase loading starts. Then, the martensite formation is activated mechanically and the martensite, which is formed with the application of stress, is called as stress induced martensite (SIM). SIM has the form of detwinned martensite structure. Thus, the shape change can be observed. Stress induced martensite transforms back to austenite when the alloy is unloaded since the martensite is not thermodynamically stable at that temperature.

Figure 2.2 shows the presence of SME and superelasticity depending on the transformation temperature ranges. There are two lines that correspond to the variation in the critical stress to create martensite and critical stresses for slip depending on temperature. Critical stress to induce SIM increases with the increase in temperature and provides a positive slope, which means that required stress for inducing martensite increases by increasing temperature. On the other hand, required stress for slip decreases with the temperature increase since the metal alloys lose their strength and their resistance to plasticity decreases. Between these lines, there are areas at which the shape memory and superelastic effect can be observed. If the stress is employed on SMA at a temperature above A_f austenite transforms to martensite and when unloading takes place martensite transforms to austenite since martensite is not stable above A_f. This is the superelasticity/pseudoelasticity effect and can be seen in the region between A_f temperature and required stress to induce martensite line. When the temperature is below A_s, the applied stress leads the transformation from austenite to martensite and the martensite may stay although the unloading takes place. Then, the strain can be regained by heating SMA beyond A_f temperature. All these can happen in the region between A_s and A_f lines, where both shape memory and superelastic effect can be realized. When SMA is loaded and unloaded below A_s temperature and the strain is recovered via heating, then this is called as SME and shown in the dotted region in Figure 2.2. Strain recovery values up to 8% are achievable with NiTi alloys by exploiting this property of SMAs [6].

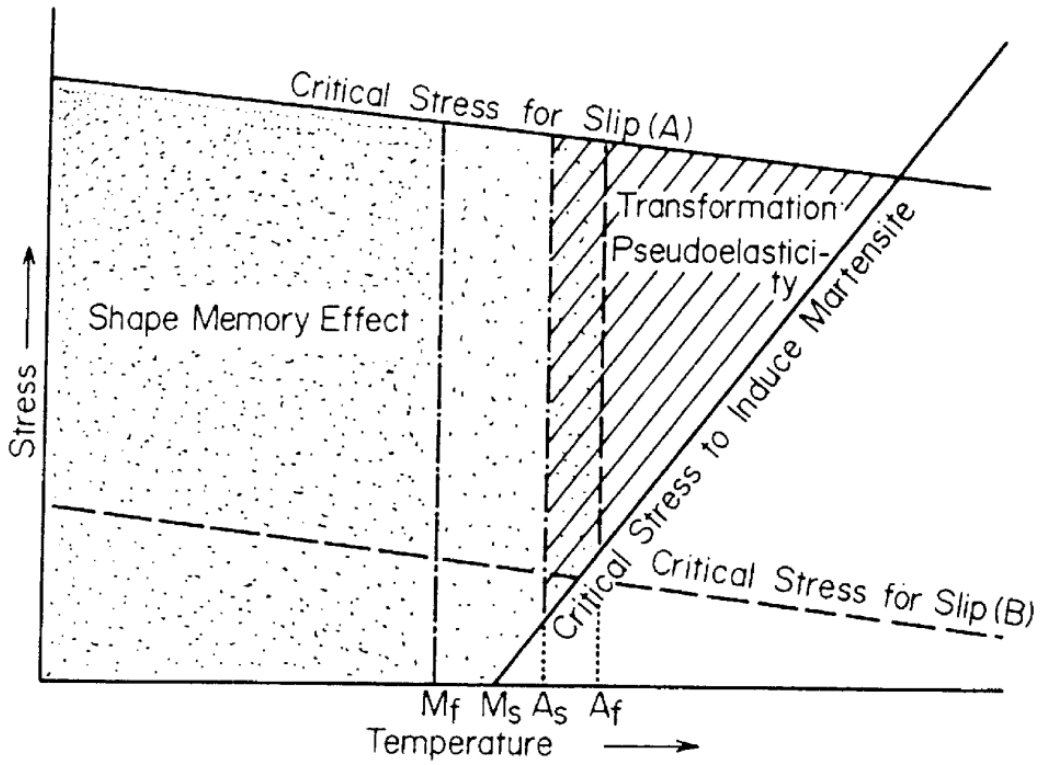

Figure 2.2. Thermo-mechanical conditions to observe shape memory and superelasticity effect [7].

2.3. Common Shape Memory Alloys

SMAs can be subdivided into three main alloying groups as Cu, Fe and Ti-based alloys. Cu and Fe based SMAs could be preferred for low-cost applications whereas Ti-based SMAs have more sophisticated usage and research area for medical and aerospace applications [8, 9].

2.3.1. Cu Based Shape Memory Alloys

Cu based SMAs are the one of the initially recognized shape memory alloys in literature [10]. Cu-Zn-Al is the most known Cu based SMA however it has quite low TTs, which are around 50°C. Cu-Zn-Al SMAs usually have susceptibility to intergranular fracture, however addition of Mn increases ductility without significantly affecting TTs. Cu-Al-Mn SMAs also have higher ductility than that of Cu-Al-Ni alloys [11, 12].

2.3.2. Fe Based Shape Memory Alloys

Iron based SMAs have promising studies in civil engineering area such as prestressing or strengthening of fatigue critic fasteners. They are able to show high transformation stress, have good weldability and low-cost properties [13, 14]. Wide variety of additional elements can be added to Fe-based SMAs such as Pt, Ni, Co, Ti, Mn, Si, C and Cr. Fe-Mn-Si SMA can be used as a fishplate in butt joints of rail profiles and joining of pipe profiles. [15].

2.3.3. NiTi Based Shape Memory Alloys

NiTi based SMAs have outstanding mechanical and actuation properties when compared to Fe and Cu based SMAs in terms of ductility and high ε_{act}. Besides these outstanding properties, biocompatibility is another exceptional property of NiTi alloys. For instance, near equiatomic binary NiTi alloys are employed as a coronary stent in angioplasty operations [16-18].

Besides the outstanding properties, which were mentioned above, TTs of NiTi alloys can be tailored. TTs of NiTi alloys decrease significantly with a small increase in Ni composition. If it is needed aging heat treatments are an effective way to increase the TTs of NiTi SMAs. Ni content in the matrix decreases when Ti_3Ni4 precipitates are formed in the matrix by aging heat treatment and as the Ni content decreases TTs increase but the TTs do not exceed 100°C [3, 19, 20]. Additionally, formation of Ti_3Ni_4 precipitates increase critical shear stress for plastic deformation via hindering formation of dislocations during superelastic (loading-unloading cycles at constant temperature) or shape memory (cooling-heating under constant stress) cycles, and therefore, cyclic stability enhances [21, 22].

However, aging heat treatments on near-equiatomic NiTi SMAs do not change TTs since precipitation does not occur according to Miyazaki's study [23].

2.4. High Temperature NiTi-Based Shape Memory Alloys

High temperature shape memory alloys are a certain group of SMAs having TTs above 100°C and abbreviated as HTSMA. Additional alloying elements should be added to NiTi binary system to increase the TTs above 100°C. Therefore, NiTi based HTSMAs may include Au, Pd, Pt, Zr or Hf alloying elements [2, 24-26]. Au, Pd and Pt are costly alloying

elements when compared with Hf and Zr, so most of the researches have been concentrated on Hf and Zr added NiTiX HTSMAs. However, NiTiZr alloys show brittleness due to their affinity to oxygen. Since HTSMAs are used as actuators at high temperatures oxidation is the main problem in Zr added NiTi alloys due to the increase in brittle behavior [27]. On the other hand, Hf alloyed HTSMAs show narrower T_{hys} and higher strength and ε_{act} which are the key properties of NiTiHf alloys for actuator applications among other NiTi based HTSMAs [20]. Therefore, Hf alloyed HTSMAs are better alternatives for HTSMA actuator applications [20, 25, 28-35].

2.5. NiTiHf High Temperature Shape Memory Alloys

Hf addition as the ternary element to NiTi SMAs has the effect of increase in TTs according to previous studies [36, 37]. Potapov's study on Ni lean $Ni_{49.8}Ti_{50.2-x}Hf_x$ alloys with x varying from 8 to 25at% shows that the TTs and T_{hys} increases with increasing Hf amount [36]. Prasher's study on Ni rich Ni50.3Ti49.7-xHfx alloys with x varying from 5 to 25at% shows that Hf additions up to 10 at% lowers the TTs with respect to the binary Ni50.3Ti49.7 composition [37]. However, further escalation in Hf concentration leads to linear increase in TTs.

Another study on Ni lean NiTiHf alloys focused on Ni/(Ti+Hf) ratio where Hf ratio is 10at% shows that brittleness occurs when Ni ratio is low [38]. Therefore, Ni rich NiTiHf alloys are more popular among HTSMA studies since mechanical, shape memory properties, cyclic stability and fatigue lifetime can be enhanced via precipitation hardening by conducting aging heat treatments. Aging heat treatment which generates $(Ti+Hf)_3Ni_4$ precipitation on Ni rich NiTiHf alloys has advantageous effects on thermal and dimensional stability and increases the strength and the TTs of the alloys. However, prolonged aging results coarsening of precipitates and hence a mitigation in the enhancement of strength and cyclic stability could be observed [39].

A study performed by Karaca et al. shows the effects of aging heat treatment on $Ni_{50.3}Ti_{29.7}Hf_{20}$ alloy by varying aging temperature between 300°C and 900°C for 3-hour aging time period. The highest TTs have been attained at 650˚C for 3 hours aged condition whereas shape memory properties were comparatively worser since precipitates were large. According to the previous studies, the aging, which was done at 550˚C for 3 hours, exhibited the satisfactory results in terms of cyclic stability and achieving the highest ε_{act}

values. The study also demonstrates that NP increased the TTs and enhanced the thermal and thermo-mechanical stability by precipitation hardening [20].

2.6. Transmission Electron Microscope (TEM) Studies on Ni-rich NiTiHf Alloys

It has been previously proved that the nano-sized precipitate formation in NiTiHf alloys by aging heat treatments improves strength and the cyclic stability [29, 40]. According to TEM, size and shapes of the NP are strongly depends on temperature. As the aging temperature increases, the precipitate size increases as well and the precipitates lose the coherency with respect to the matrix. 3h aging at 550°C formed coherent NP in Ni50.3Ti29.7Hf20 alloy as shown in Figure 2.4 and these precipitates raised the strength and enhanced the cyclic stability together with the fatigue life of Ni50.3Ti29.7Hf20 alloy [35].

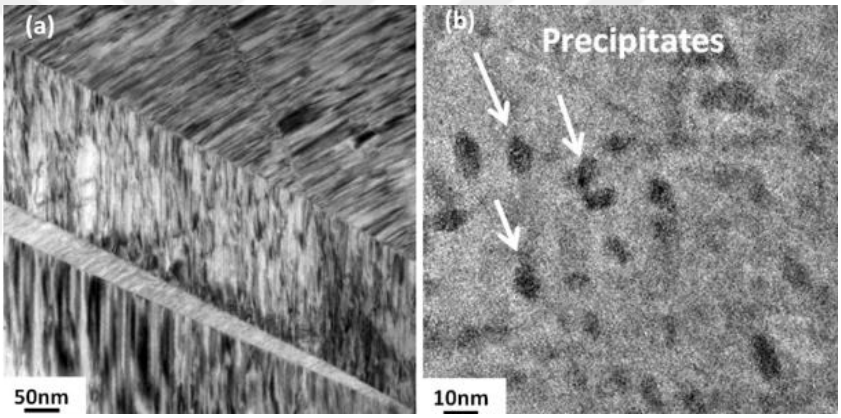

Figure 2.3. TEM Images of (a) the extruded Ni50.3Ti29.7Hf20 TEM sample revealing internal twins, (b) the Ni50.3Ti29.7Hf20 sample that was aged for 3h at 550°C with NP [35]

Figure 2.3.(a) and (b) show TEM images of the solutionized and the aged Ni50.3Ti29.7Hf20 alloy from another study [40]. The aging condition was the same as was in the study aforementioned above. The solutionized sample, shown in Figure 2.4.(a) does not contain any precipitates and comprises a single B2 austenite phase which can be corroborated by the SAD pattern (attached to Figure 2.4.(a)). SAD pattern does not indicate any evidence of additional detail or evident for the existence of a second phase. Whereas 3h aging at 550°C formed oblate spheroid shaped fine precipitates having size approximately 15–20 nm as shown in Figure 2.4.(b). The precipitates were named as H-

phase in the literature, which has been previously stated for Ni-rich NiTiHf alloys [40]. In the same study, it was shown that, as the aging temperature was increased from 550°C to 650°C, the precipitate size became larger and the hardening due to aging began to disappear [40].

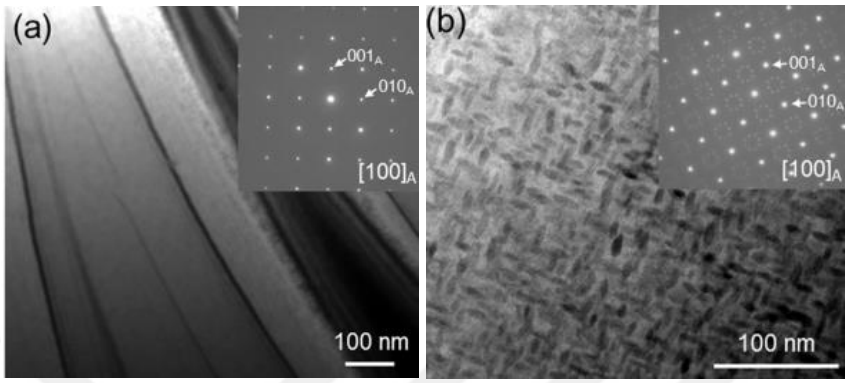

Figure 2.4. TEM Image of (a) the solutionized sample and (b) the sample, which was aged for 3h at 550°C [40].

2.7. Effect of Severe Deformations on NiTi based SMA

In order to improve cyclic stability and strength of the of SMAs, critical shear stress for slip must be increased. High number of dislocations can be induced by conventional or Severe Plastic Deformation (SPD) processes such as cold-rolling, extrusion, drawing and equal channel angular extrusion (ECAE) [28]. Severe deformations that are done at ambient temperature lead to an increase in number of dislocations which inhibits the formation of new dislocations during martensite-austenite phase transformations [41]. Therefore, thermal, and thermo-mechanical cyclic stability improves due to higher dislocation density, but TTs drop since overcooling should be applied for austenite to martensite phase transformation [28, 41-44]. The study of Karaman's group on $Ni_{50}Ti_{30}Hf_{20}$ HTSMA about the influence of warm rolling and cold rolling with subsequent annealing processes has showed improvement on the cyclic stability with the rolling and annealing processes and gave promising results for high temperature actuator applications [41]. Additionally, Kockar's group revealed that the TTs of $Ni_{50.3}Ti_{29.7}Hf_{20}$ SMA also became stable by either aging after cold rolling or aging after hot extrusion. After all, aging of CR $Ni_{50.3}Ti_{29.7}Hf_{20}$ SMA is an alternative process to enhance the TTs and the dimensional stability via lowering irrecoverable strain as well [4].

2.8. Effect of Stress Assisted Aging on NiTi based SMA

Unlike conventional stress-free aging, stress aging is a type of aging heat treatment that is done under either constant compressive or tensile stresses which directly affects precipitate orientation and distribution in the alloy matrix. When aging under stress is done, certain precipitates are aligned through the applied stress direction which might be favourable to enhance shape memory properties. In Radi's study, fewer variants of precipitates have been observed in stress aged Ni-rich NiTi alloy. Moreover, stress aging has limited the length of precipitates and increased Ms temperature according to this study [22]. Another study done on NiTiHfPd SMA by E.Acar et al., has showed similar results about fewer precipitate variant formation [45].

2.9. Functional Fatigue of Shape Memory Alloys

Although SMAs are candidates of future mechanical actuator applications their utilization is restricted by the fatigue failures. Conventional structural materials such as steel, aluminium etc. have well known for suffering from structural fatigue issues. SMAs can exhibit two separate fatigue failure modes, which are structural fatigue failure (as seen in conventional metals and metal alloys) and functional fatigue (FF). FF is defined as the loss of shape memory or superelastic properties with the number of heating-cooling or loading-unloading cycles, respectively and dimensional stability diminishes at each cycle. Composition of alloy, heat treatment or mechanical treatments such as aging or cold working dictate the functional fatigue life (FFL) and functional fatigue behaviour (FFB) of all SMAs as well as Ni-rich Ni(50.3at%)Ti(30at%)Hf(20at%) SMA, which was examined in this study.

3. EXPERIMENTAL PROCEDURE

3.1. Summary of Workflow

There have been many aging and deformation studies, which were conducted on Ni-rich Ni(50.3at%)Ti(30at%)Hf(20at%) SMAs. However, most of them focused on just aging of the alloy without applying stress and just the effect of rolling on the shape memory properties. In this study, the combined effect of cold rolling with successive stress assisted aging was investigated. In Figure 3.1, the experimental route, which was followed in this study, is shown. Firstly, workflow starts with receiving the alloy in as cast round bar condition.

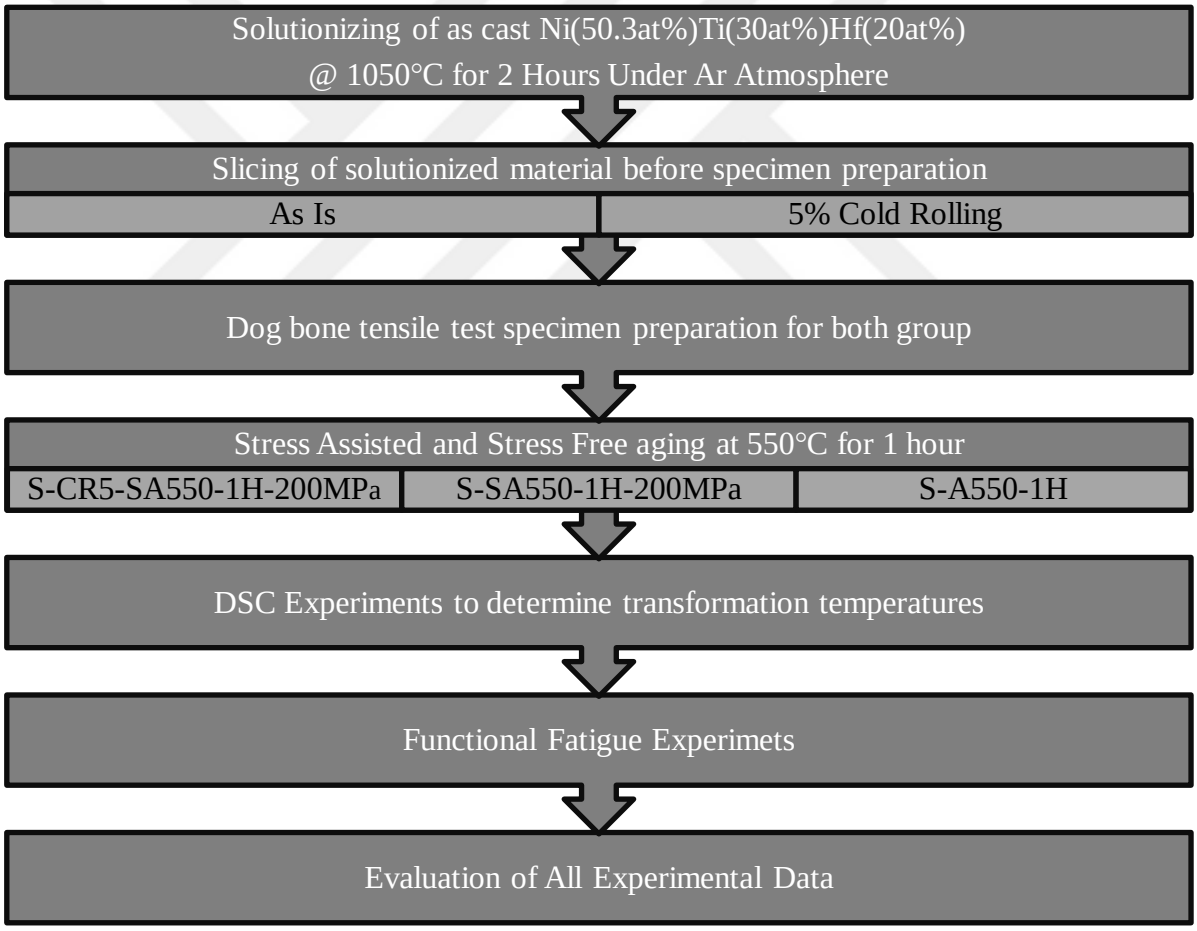

Figure 3.1. Experimental workflow of the study.

All the samples were solutionized at 1050°C for 2 hours before the cold rolling and aging treatments. Then, slices were cut from the solutionized alloy for aging, stress assisted

aging and cold rolling with successive stress assisted aging processes. Description of the thermal and thermo-mechanical treatments, which were applied to Ni(50.3at%)Ti(30at%)Hf(20at%) alloy and the corresponding abbreviations, which were used in this study are presented in Table 3.1. It must be stated that the shape memory and functional fatigue properties of solutionized sample were determined in a previous study and used in this study for comparison [46].

Firstly, TTs of S-CR5-SA550-1H-200MPa, S-SA550-1H-200MPa and S-A550-1H samples were measured using DSC technique. Then, FFEs were performed on all thermo-mechanically treated samples under 200MPa constant tensional stress. After FFEs, ε_{mar}, ε_{aus} and ε_{act} versus the transformation temperature graphs were derived from the strain vs temperature graphics obtained from the FFEs to determine the effect of thermal, mechanical and thermomechanical heat treatments. The applied treatments are further explained in latter sections.

Table 3.1. Thermal and Thermo-mechanical Conditions that were applied and the corresponding abbreviations which were used in this study.

Abbreviations	Description of Material Condition
S-CR5-SA550-1H-200MPa	Solutionized + 5% Cold Rolled + Stress Aged @ 550°C for 1 hour under 200 MPa tension stress
S-SA550-1H-200MPa	Solutionized + Stress Aged @ 550°C for 1 hour under 200 MPa tension stress
S-A550-1H	Solutionized + Aged @ 550°C for 1 hour
S	Solutionized (Solution Heat Treated)

3.2. Solutionizing

Solutionizing is a heat treatment method to dissolve all principal alloying constituents into a solid solution and generally applied to homogenize the chemistry of the alloys. Solutionizing was performed at 1050°C for a duration of 2 hours to obtain a homogeneous solid solution and chemistry before aging heat treatment. Since NiTiHf is a very oxidative alloy time duration was kept as low as 2 hours and the alloy was wrapped with a tantalum foil and the solutionizing was conducted under Argon atmosphere to prevent severe oxidation at high temperature.

3.3. Slicing

Solutionized alloy was sliced into plates with 1.05mm thickness by Wire Electron Discharge Machine (WEDM) and WEDM residue was smoothly ground prior to cold rolling process.

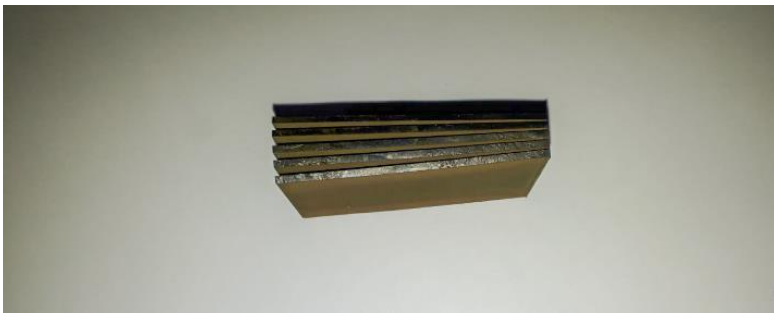

Figure 3.2. Sliced Ni(50.3at%)Ti(30at%)Hf(20at%) alloy.

3.4. Cold Rolling

Cold rolling is a mechanical treatment usually done to produce sheet metals/metal alloys and also to increase the strength by creating residual compressive stress and dislocations. However, effect of cold rolling might be limited to the thin layers near the upper and lower surfaces rather than full cross-section depending on the thickness and depending on the thickness reduction. NiTiHf slices was CR at room temperature by the machine shown in Figure 3.3 at room temperature.

Figure 3.3. Laboratory type cold rolling machine.

3.5. Dog Bone Specimen Preparation for Functional Fatigue Experiments

Dog bone shaped samples were cut by WEDM to prevent unexpected transformation due to released heat with conventional machining. Machining also induces residual stresses on machined parts, which might adversely affect the TTs of the SMAs. However, WEDM residues are present on the samples.

Therefore, WEDM residues were eliminated by smooth grinding and the surface of the tensile samples were examined with optical microscope to control possible micro crack formations on the surfaces. The drawing of the dog bone shaped tensile test samples is shown in Figure 3.4. Lastly, narrow segment of the specimens was painted with temperature resistant black spray paint for contactless temperature measurement via using laser pyrometer.

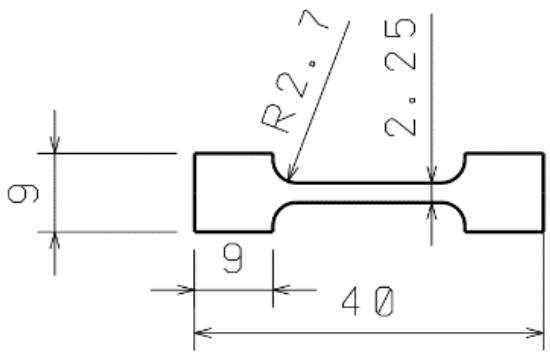

Figure 3.4. 2D technical drawing of test specimen, dimensions are in mm.

3.6. Stress Free Aging

Aging heat treatment is a process to create precipitates within most of the age hardenable metal alloys such as Aluminium, Titanium and Magnesium alloys. To perform stress free aging, a tube furnace (see Figure 3.5) was heated up to the 550°C aging temperature and waited for a time for temperature stabilization. Then, S (Solutionized) specimens were placed into vertical tube furnace and the chamber of the furnace was purged with Argon to prevent a possible oxidation. Finally, specimens were cooled rapidly to maintain the aged microstructure.

Figure 3.5. Vertical Tube Furnace for conducting solutionizing and aging heat treatments.

3.7. Stress Assisted Aging

Stress assisted aging is a special type of aging heat treatment where material is exposed to stress during aging process. Since vertical tube furnace is mechanically inconvenient to load the specimen during aging, FFE test setup was used for stress assisted aging processes. A schematic representation of FFE test setup is shown in Figure 3.6. The samples were aged by Joule Heating method at 550°C temperature and loaded to 200MPa. The time duration was chosen as 1 hr to prevent severe oxidation of the samples during stress assisted aging treatment since the process can be done only in open atmosphere.

3.8. Functional Fatigue Experiments (FFE)

Functional fatigue experiments (FFEs) have been executed with a test setup built by off-the shelf equipment, which is shown in Figure 3.6. Samples were heated via using Joule Heating method whereas cooling was provided by pressurized air with nozzles.

Temperature and speed of heating-cooling were controlled by National Instrument (NI) PID controller. The feedback for this control was gathered from contactless laser

pyrometer that is Optris CTlaser LTF-CF1 to control DC power supply and air regulator valve. Additionally, the Upper and Lower Cycle Temperatures, which will be presented as UCT and LCT throughout the text were also set to constant values to the controller since especially UCT is a very important parameter, which dictates the fatigue lifetime of the alloys. If UCT is kept very high the alloys can creep at high temperatures and less fatigue life can be achieved, if it is kept low then full austenitic transformation cannot be attained. Static load application was done by hanging dead weights to the samples. The magnitude of the load was calculated to achieve the required stress to apply to the specimen.

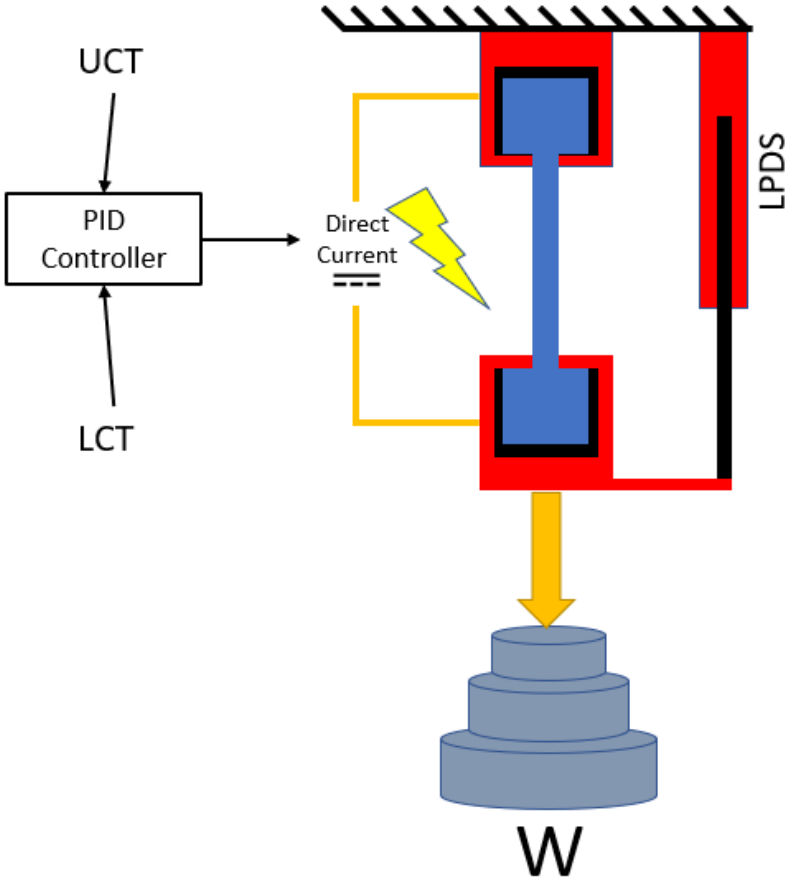

Figure 3.6. Schmeatic representation of FFE Test Setup.

Displacement of the specimen was measured with a Linear Potentiometer Displacement Sensor (LPDS). Displacement together with the temperature data were recorded to draw strain vs. temperature graphics to analyse the functional fatigue properties of the thermally and thermo-mechanically treated alloys. All the TTs, which are A_f, A_s, M_s M_f,

T_{hys} together with the ε_{mar}, ε_{aus} and ε_{act} values were drawn from Strain vs Temperature graphics following the route that is defined in Figure 3.7.

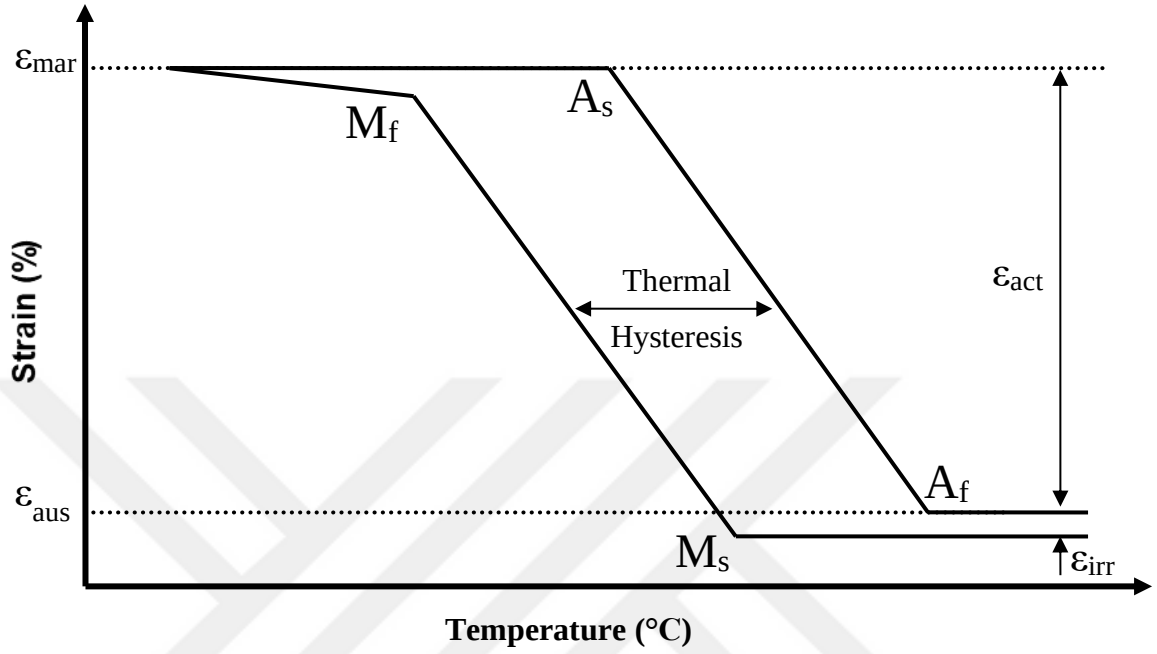

Figure 3.7. A schematic representation of strain vs temperature behaviour of SMA under tensile load.

3.9. Differential Scanning Calorimetry (DSC)

Perkin Elmer 8000 DSC was utilized to measure the TTs of all samples in this study. DSC 8000 is able to directly measure the heat flow of the sample in a predetermined temperature range since it has a double furnace system. SMA sample and the reference sample are put into separate furnaces and the power can be adjusted with a closed loop system. The heat power to the furnace in which the SMA is placed is adjusted to cycle measured sample three times between 0°C and 300°C with 10°C/min temperature variation rate.

Figure 3.8. Perkin Elmer 8000 DSC device.

4. EXPERIMENTAL RESULTS AND DISCUSSION

4.1. Differential Scanning Calorimetry (DSC) Results

First of all, the TTs of all samples were investigated using DSC via running three thermal cycles with 10°C/min heating-cooling rate. Second heating-cooling cycles of DSC results of S-A550-1H, S-SA550-1H-200MPa and S-CR5-SA550-1H-200MPa Ni(50.3at%)Ti(30at%)Hf(20at%) samples were shown in Figure 4.1., Figure 4.2. and Figure 4.3., correspondingly. Tangent method was used to determine TTs from the DSC curves. DSC experiment was previously conducted on Solutionized Ni(50.3at%)Ti(30at%)Hf(20at%) sample and the results were published before [4, 46]. TTs, which were gathered from all three cycles, are tabulated separately for Solutionized (S), S-A550-1H, S-SA550-1H-200MPa and S-CR5-SA550-1H-200MPa Ni(50.3at%)Ti(30at%)Hf(20at%) samples in, Table 4.1., Table 4.2. and Table 4.3., correspondingly. The differences between the last and first thermal cycles are also presented in terms of Max. ΔT for these samples to mention the stability of TTs through stress free thermal cycles. Generally speaking, all the TTs of all samples including Solutionized one were determined to be quite stable in DSC cycles. Please note that the results of S sample were taken from the DSC curves in Ref [46].

To better track the evolution of the TTs on stress-free, stress-assisted aged and CR with successively stress-assisted aged treatments, TTs of all samples including the Solutionized (S) sample, which were extracted from the 2^{nd} heating cooling cycles of DSC experiments are shared in Table 4.5. Additionally, the enthalpy values of the transformations of all samples are qualitatively compared in Figure 4.4. It should be noted that enthalpy values can be calculated by taking the areas under the transformation peak, which are clearly seen in DSC curves. Enthalpy values can be directly related with the volume of the martensite-austenite (during heating) and austenite-martensite (during cooling) transformations.

Table 4.1. TTs of Solutionized (S) Sample, which were determined from DSC curves

Solutionized (S)	M_f [°C]	M_s [°C]	A_s [°C]	A_f [°C]
1st cycle	155.9	165.3	188.4	196.6
2nd cycle	153.3	163.1	180.8	190.6
3rd cycle	152.4	161.7	178.4	186.9
Max. ΔT	3.5	3.6	10	9.7

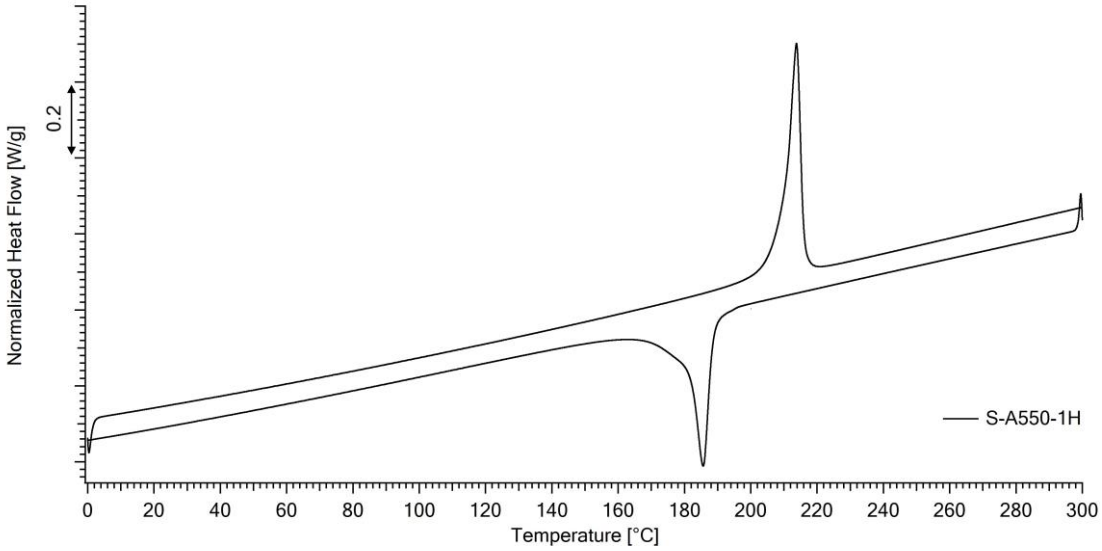

Figure 4.1. Second heating-cooling cycle of DSC experiment for S-A550-1H sample.

Table 4.2. TTs of S-A550-1H Sample, which were determined from DSC curves.

S-A550-1H	M_f [°C]	M_s [°C]	A_s [°C]	A_f [°C]
1st cycle	182.4	190	210	217
2nd cycle	180.9	189.2	206.1	216.5
3rd cycle	179.2	188.4	204	215.4
Max. ΔT	3.2	1.6	6	1.6

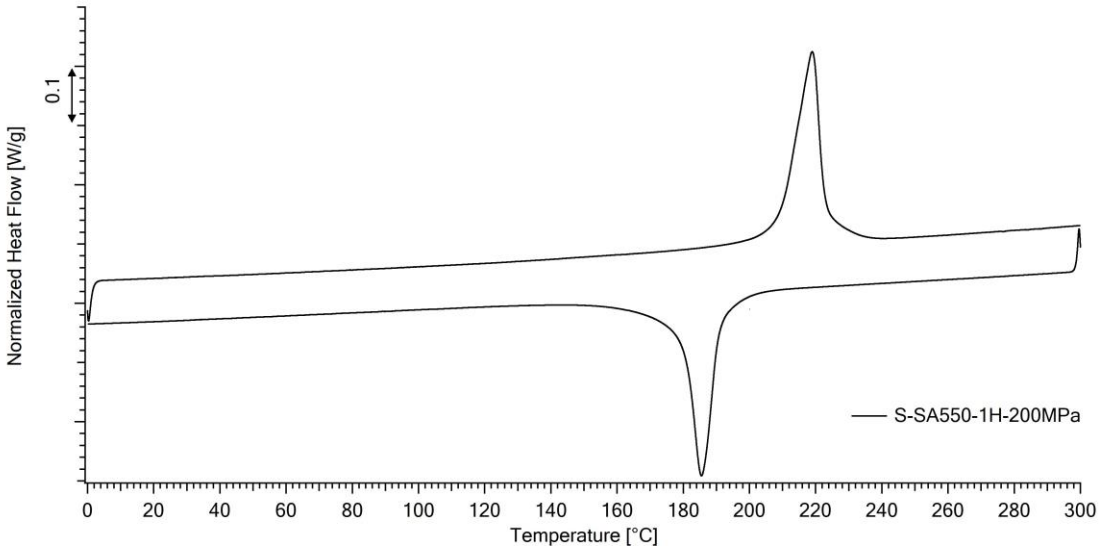

Figure 4.2. Second heating-cooling cycle of DSC experiment for S-SA550-1H-200MPa sample.

Table 4.3. TTs of S-SA550-1H-200MPa Sample, which were determined from DSC curves.

S-SA550-1H-200MPa	M_f [°C]	M_s [°C]	A_s [°C]	A_f [°C]
1st cycle	183	193	219	228
2nd cycle	180.3	191.5	209	223.1
3rd cycle	180	190	209	223
Max. ΔT	3	3	10	5

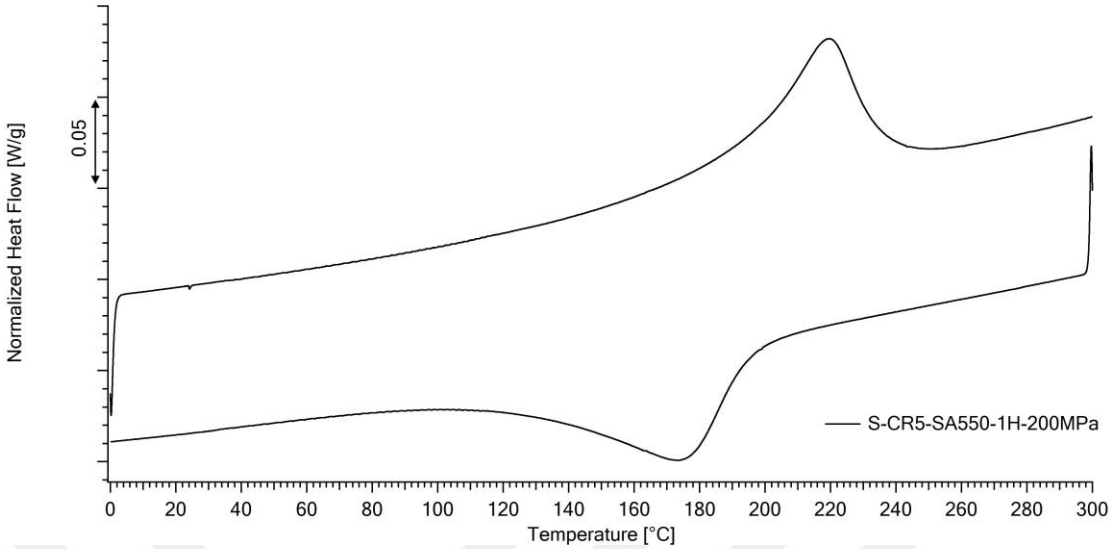

Figure 4.3. Second heating-cooling cycle of DSC experiment for S-CR5-SA550-1H-200MPa sample.

Table 4.4. TTs of S-CR5-SA550-1H-200MPa Sample, which were determined from DSC curves.

S-CR5-SA550-1H-200MPa	M_f [°C]	M_s [°C]	A_s [°C]	A_f [°C]
1st cycle	130	196	203	240
2nd cycle	123.4	195.7	198.6	236.2
3rd cycle	127	194	193	235
Max. ΔT	3	2	10	5

As aforesaid, transformation enthalpies of all samples are qualitatively compared at Figure 4.5. It could be deduced from the comparison of the DSC curves, the transformation enthalpies, in other words, the areas under the transformation peaks decreased with the application of stress aging and cold rolling (CR) with successive stress aging processes due to the precipitation formation with the dislocation density increase. Please note that, the transformation enthalpies can be correlated with transforming volume. Precipitates do not show martensite-austenite transformation, therefore, the transforming volume was decreased in the samples, which were stress assisted aged and CR with successively stress assisted aged.

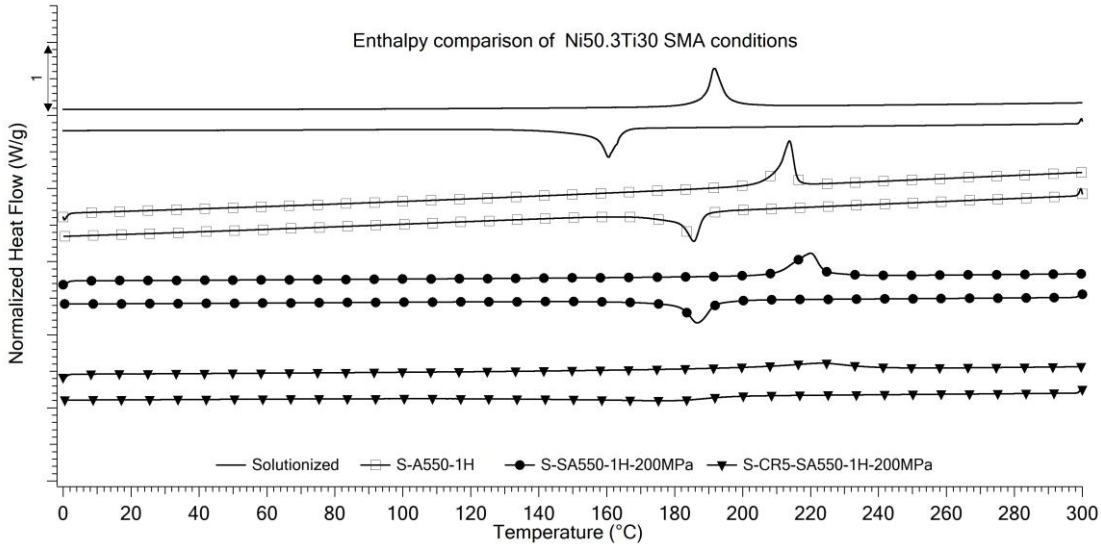

Figure 4.4. Transformation Enthalpy comparison the Solutionized (S), S-A550-1H, S-SA550-1H-200MPa and S-CR5-SA550-1H-200MPa Ni(50.3at%)Ti(30at%)Hf(20at%) samples.

As shown in Table 4.5, TTs increased as a result of aging for 1 hour at 550°C, whether the aging process was performed under stress or not. It was only observed that aging under stress had quite a small effect on the change of TTs since almost no difference was observed between the TTs of S-A550-1H and S-SA550-1H-200MPa samples. It can be deduced from the results that formation of NP caused a drop in the Ni-amount of the matrix, therefore the TTs increased [4, 20]. Moreover, the sample, which was CR and the stress aged at 550°C under 200MPa for 1 hr, also showed approximately the same Ms, As and Af temperatures with the S-SA550-1H-200MPa sample. One can observe only a

significant decrease in the Mf temperature of S-CR5-SA550-1H-200MPa sample with respect to other aged samples. As can be seen from the second cycle DSC curve of S-CR5-SA550-1H-200MPa sample in Figure 4.3, the transformation peak of the cooling curve is not sharp. Martensitic transformation was completed in this sample in a wide temperature range so the difference between Ms and Mf was determined as so large. This can be attributed to the dislocations, which hinder the martensite boundary movement in the austenite phase by pinning the martensite-austenite phase boundaries. Hence, more undercooling is necessary to overcome this pinning effect of dislocations. It was previously reported in the literature that even transformation peaks are not observed in CRed SMAs due to the dislocations. In this study, the influence of cold rolling may be a little recovered during aging the samples at 550°C for 1 hour under stress with the annihilation or rearrangement of the dislocation forests.

Table 4.5. TTs drawn from the 2nd cycle DSC curves of (S), S-A550-1H, S-SA550-1H-200MPa and S-CR5-SA550-1H-200MPa Ni(50.3at%)Ti(30at%)Hf(20at%) samples.

	M_f	M_s	A_s	A_f
S	153.3	163.1	180.8	190.6
S-A550-1H	180.9	189.2	206.1	216.5
S-SA550-1H-200MPa	180	190	209	223
S-CR5-SA550-1H-200MPa	127	194	193	235

4.2. Functional Fatigue Experiments (FFE)

FFEs were performed under 200 MPa tensile stress on S-A550-1H, S-SA550-1H-200MPa and S-CR5-SA550-1H-200MPa Ni(50.3at%)Ti(30at%)Hf(20at%) samples. It is important to mention that FFE on S sample was previously conducted and published before [4, 46]. UCT temperature was set to approximately 350°C to achieve full austenite transformation. Strain vs Temperature curves were drawn for all FFEs and all TTs, ε_{mar}, ε_{aus} and ε_{act} values were drawn from the curves and demonstrated as a function of cycles in this part of the study. The procedure, which was followed to find out the aforesaid shape memory properties, was previously shown in Figure 3.7.

4.2.1. FFE Results of S-A550-1H Sample

Strain-Temperature curves that were drawn using FFE data of S-A550-1H sample are demonstrated in Figure 4.5. T_{hys} are also shown on the curves as well. Figure 4.5 shows strain- temperature curves shifted to the higher temperatures with the number of cycles (NC) since dislocations were stored at each cycle and thus, the full transformation to austenite was achieved at relatively higher temperatures. Additionally, the slope of the heating and cooling curves decreased. This is also the indication of the proliferation in dislocation density by the increasing of NC. As a consequence of the increase in dislocation density, more heating and cooling were necessary for the complete austenite and martensite transformations.

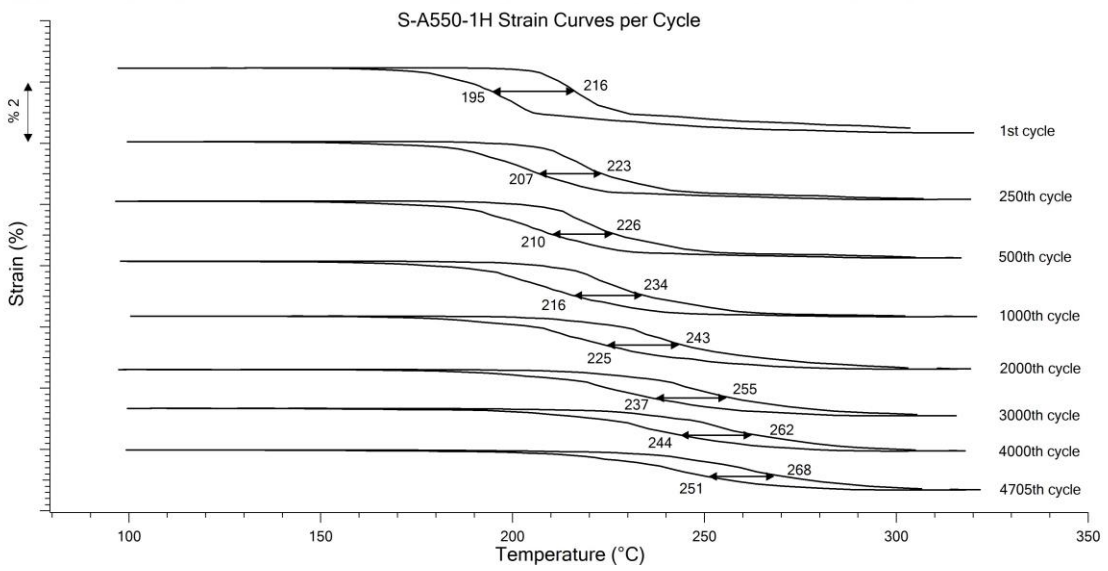

Figure 4.5. Strain-Temperature curves, which were obtained from FFE of S-A550-1H sample range per Cycle

Figure 4.6 shows ε_{mar}, ε_{aus} and ε_{act} values, which were drawn from Figure 4.5. S-A550-1H sample failed at 4705 cycles. Please note that, ε_{aus} corresponds to accumulated irrecoverable strain (AIS) in FFEs. Irrecoverable strains from each cycle are added up to determine the AIS as a function of cycle. It can be deduced from Figure 4.6 that ε_{act} values decreased as the ε_{aus}, in other terms, AIS increased. The decrease in ε_{act} with the NC is an expected behaviour since as the dislocation density increases full recovery of the shape change cannot be attained due to the pinning of martensite boundaries with the dislocations. Plastic deformation and the retained martensite volume increase.

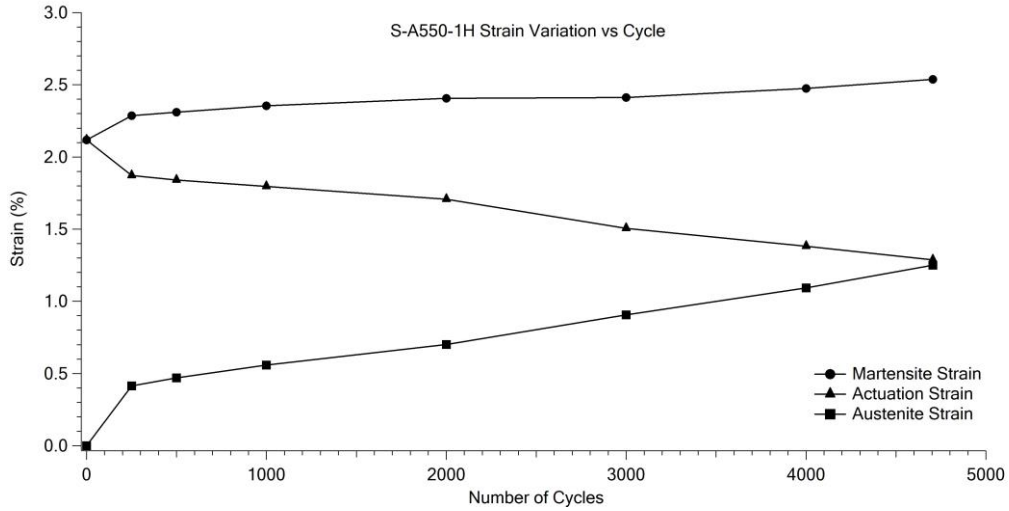

Figure 4.6. ε_{mar}, ε_{aus} and ε_{act} Values as a function of cycles, which were extracted from Strain-Temperature curves of S-A550-1H sample.

Figure 4.7. and Table 4.6. show variation of TTs as a function of cycles until the fracture. All the TTs increased by the NC due to the necessity of overcoming dislocation pinning effect. At higher temperatures, the dislocations become more mobile and they do not pin the martensite-austenite boundary and the martensite-austenite phase boundary becomes mobile.

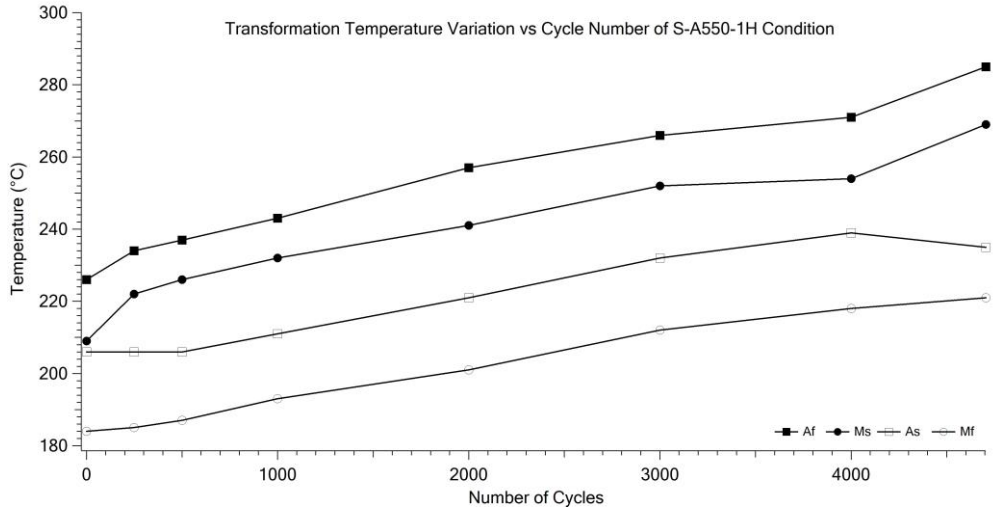

Figure 4.7. Transformation Temperature Values, which were extracted from Strain-Temperature curves of S-A550-1H sample.

Table 4.6. Transformation Temperature Values with the cycle numbers, which were extracted from Strain-Temperature curves of S-A550-1H sample.

Cycle #	Mf (°C)	Ms (°C)	As (°C)	Af (°C)
1	184	209	206	226
250	185	222	206	234
500	187	226	206	237
1000	193	232	211	243
2000	201	241	221	257
3000	212	252	232	266
4000	218	254	239	271
4705	221	269	235	285
Δt	37	60	33	59

4.2.2. FFE Results of S-SA550-1H-200MPa Sample

Strain-Temperature curves, which were gathered from the FFE of S-SA550-1H-200MPa sample, are presented in Figure 4.8.

Figure 4.9. shows ε_{mar}, ε_{aus} and ε_{act} results of FFE of S-SA550-1H-200MPa sample. Specimen failed at 2250 cycles and AIS reached to a value of approximately 2 %. Additionally, ε_{act} decreased from 2.9% down to approximately 2% values till the failure. Higher actuation and AIS values led to observe early failure.

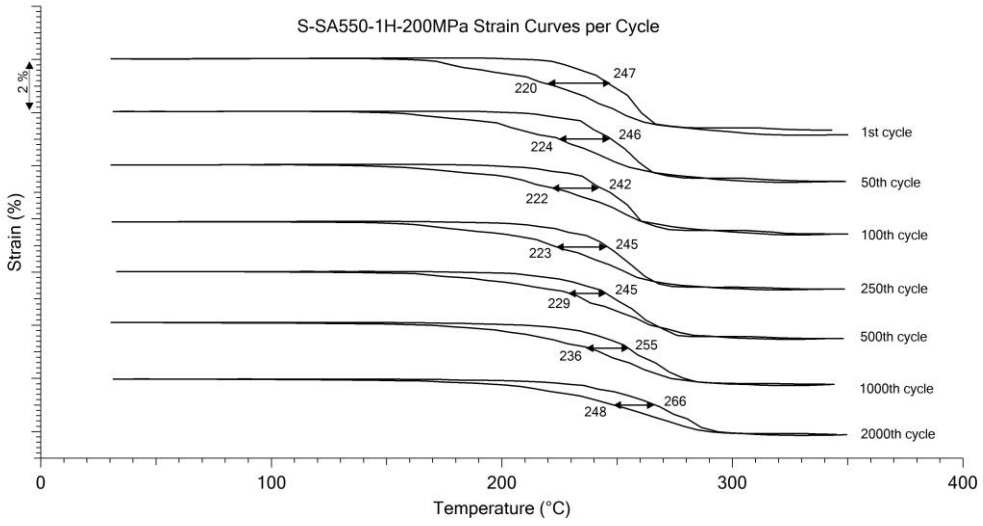

Figure 4.8. Strain-Temperature curves, which were obtained from FFE of S-SA550-1H - 200MPa sample.

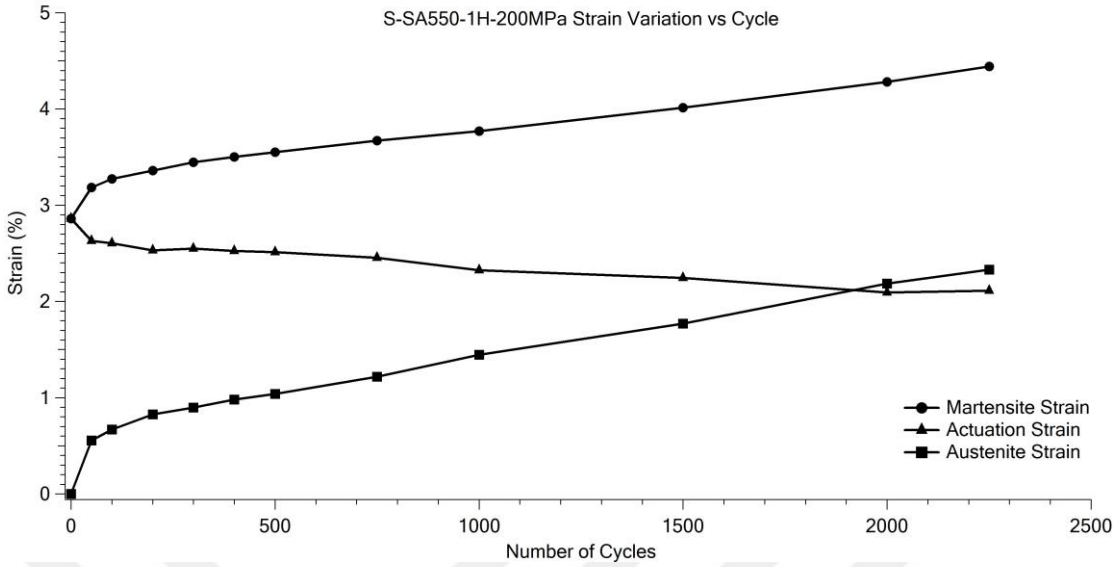

Figure 4.9. ε_{mar}, ε_{aus} and ε_{act} Evolution as a function of cycles, which were extracted from Strain-Temperature plot of S-SA550-1H-200MPa sample.

TT evolution of S-SA-1H-200MPa sample with the NC is exhibited in Figure 4.10. and Table 4.7. There are two intriguing findings, which can be drawn from TT results of this sample. All the transformation temperatures were determined to be more stable throughout the FFE. Moreover, M_s temperatures were measured to be as high as A_f temperature. The reason of measuring higher M_s temperature than that of A_s temperature was previously explained in the literature and this was attributed to the internal stresses, which can be created with applying stress or deformation processes and/or creating nano precipitates, may help the martensitic transformation to take place earlier during cooling the sample from austenite. In this study, M_s temperatures of all samples, which were measured during FFEs, were determined to be higher than the A_s due to the internal stresses which were possibly induced via aging, aging under stress and cold rolling processes.

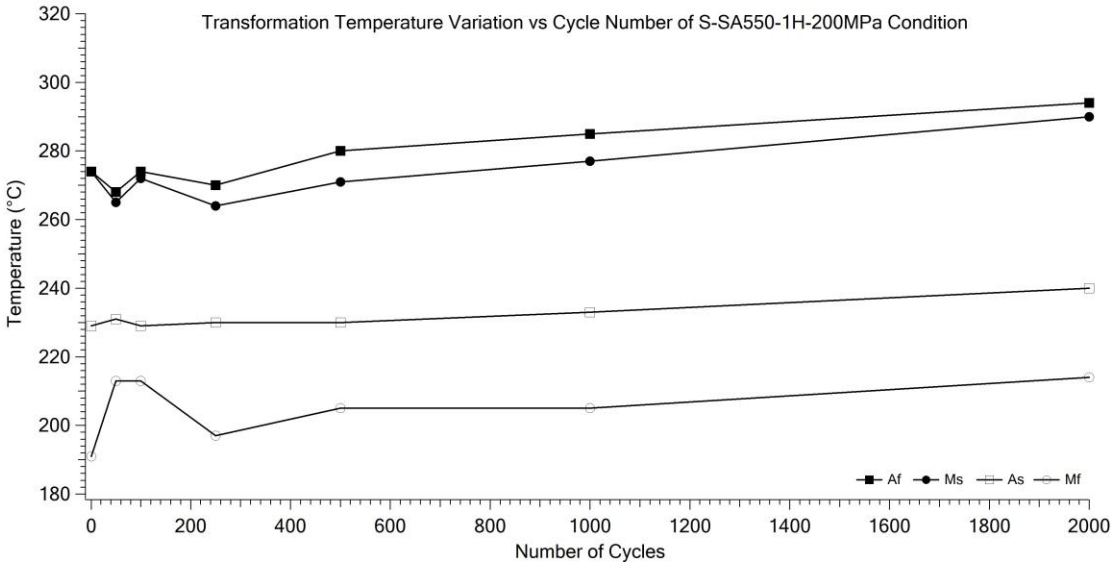

Figure 4.10. Transformation Temperature Values, which were drawn from Strain-Temperature Figure 4-10 curves of S-SA550-1H-200MPa sample.

Table 4.7. Transformation Temperature Values with the cycle numbers, which were drawn from Strain-Temperature curves of S-SA550-1H-200MPa sample.

Cycle #	Mf (°C)	Ms (°C)	As (°C)	Af (°C)
1	191	274	229	274
50	213	265	231	268
100	213	272	229	274
250	197	264	230	270
500	205	271	230	280
1000	205	277	233	285
2000	214	290	240	294
Δt	23	26	11	26

4.2.3. FFE Results of S-CR5-SA550-1H-200MPa Sample

Figure 4.11. shows Strain-Temperature curves and T_{hys} on temperature axis, which were obtained from FFE of S-CR5-SA550-1H-200MPa sample. Transformation temperature shift is very prominent at the beginning and the heating-cooling curves are very shallow.

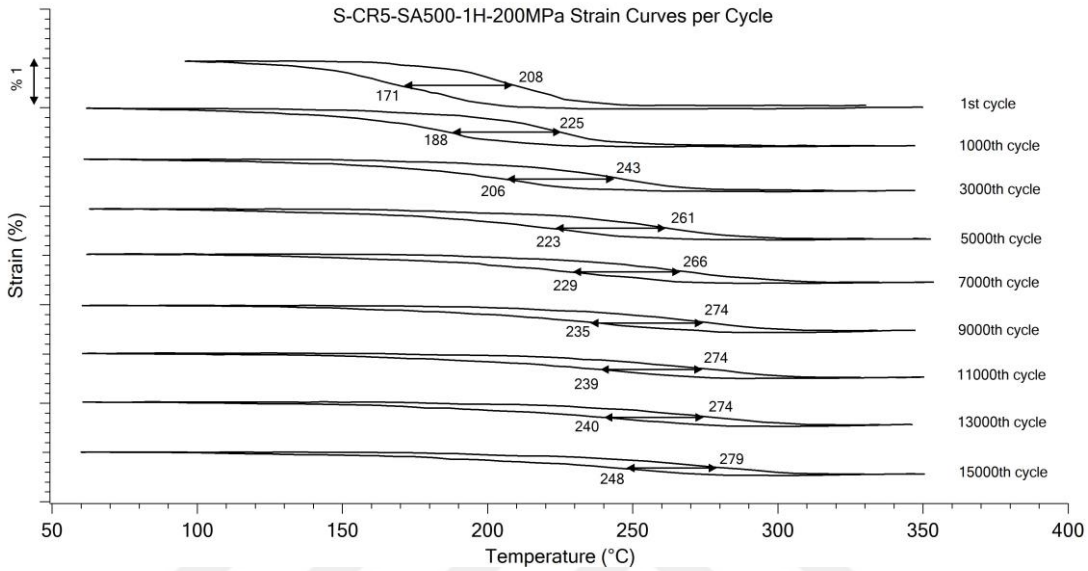

Figure 4.11. Strain-Temperature curves, which were obtained from FFE of S-CR5-SA550-1H-200MPa sample.

Figure 4.12. shows ε_{mar}, ε_{aus} (AIS) and ε_{act} results of the S-CR5-SA550-1H-200MPa sample, which were drawn from the Figure 4.24. Experiment had to be stopped at 15000 cycles due to the decrease in the thickness of the sample so displacement could not be measured after then.

AIS determined as 0.6 % at the end of the FFE. On the other hand, the ε_{act} values were very low as well compared with S-A550C-1H and S-CR5-SA550C-1H samples since the dislocations induced by cold rolling supress transformation and the transforming volume decreases. The decrease in enthalpy, which was expressed in DSC results of S-CR5-SA550-1H-200MPa also confirms the decrease in transforming volume.

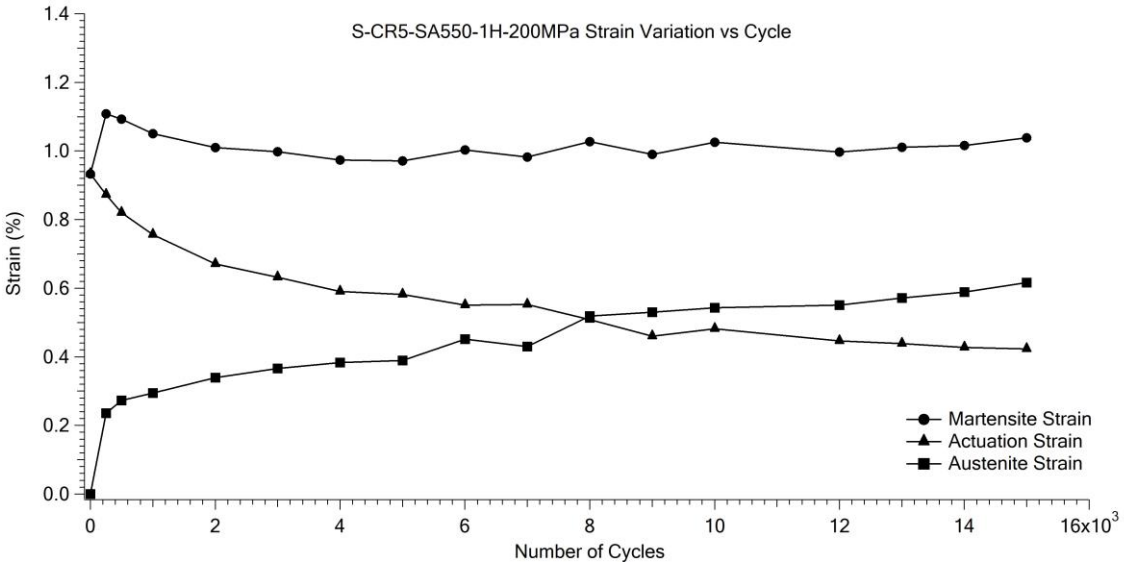

Figure 4.12. ε_{mar}, ε_{aus} and ε_{act} values as a function of cycles, which were extracted from Strain-Temperature plot of S-CR5-SA550-1H-200MPa Sample.

Figure 4.13. and Table 4.8. on the following page show the evolution of TTs till the end of FFE. TTs increased at the beginning and almost stabilized at 9000th cycle.

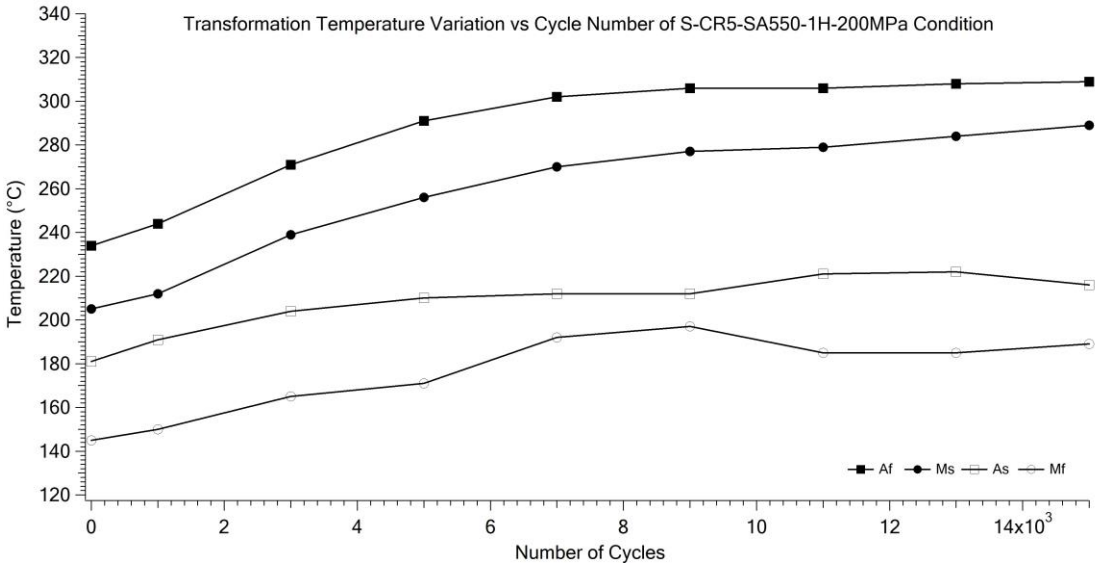

Figure 4.13. Transformation Temperature Values, which were drawn from Strain-Temperature curves of S-CR5-SA550-1H-200MPa Sample

Table 4.8. Transformation Temperature Values with the cycle numbers, which were drawn from Strain-Temperature curves of S-CR-SA550-1H-200MPa sample.

Cycle #	M_f (°C)	M_s (°C)	A_s (°C)	A_f (°C)
1	145	205	181	234
1000	150	212	191	244
3000	165	239	204	271
5000	171	256	210	291
7000	192	270	212	302
9000	197	277	212	306
11000	185	279	221	306
13000	185	284	222	308
15000	189	289	216	309
Δt	52	84	41	75

4.3. Comparison of FFE Results of all Samples

To clearly examine effects of stress-free and stress-assisted aging and cold-rolling with successive stress-assisted aging processes on SME and functional fatigue properties of Ni(50.3at%)Ti(30at%)Hf(20at%) alloy, all the FFE results of S-A550-1H, S-SA550-1H-200MPa and S-CR5-SA550-1H-200MPa samples were examined carefully with the FFE results of the base sample condition, which was the solutionized one. The FFE results of the Solutionized sample were taken from the previous study [46] and used in this thesis.

4.3.1. Transformation Temperature Comparison

The evolutions of A_s, A_f, M_s and M_f temperatures of all samples with the NC are compared in Figure 4.14 to Figure 4.17 respectively. Here are the main findings, which can be drawn from the TT evolution graphics.

1) A_s and A_f temperatures of the S sample first decreased and then started to increase after 300 and 100 cycles, respectively. Almost all the other samples showed an increasing tendency in A_s and A_f values through the end of the cycles.
2) M_s temperatures of all samples increased by the NC and M_f temperatures of just the solutionized sample dropped at the beginning of FFE and then it increased right after 500^{th} cycle. The rest of the samples showed increasing tendency in M_f temperature as well.
3) A_s, A_f and M_s temperatures of S-A550-1H, S-SA550-1H-200MPa and S-CR5-SA550-1H-200MPa samples were identified to be always higher than S sample

from the beginning of the FFEs. However, since the rate of the increase in the TTs of the S sample was very high, the TTs of the S Sample exceeded the others later during FFE.

As a summary, except the solutionized sample, TTs of all the other sample demonstrated an increasing tendency in FFEs. Actually, a decrease at the first couple of hundred cycles was observed in S sample and then a tremendous increase in all TTs of S sample was observed. Shifting of TTs to higher values is an expected phenomenon since dislocation storage with the NC leads to pinning of mobile martensite-austenite phase boundaries and higher heat input is necessary to overcome the pinning effect such that the martensite-austenite transformation can continue. Additionally, the tremendous increase in the TTs or in other words, the rapid increase of the TTs of S sample in its short fatigue life can be attributed to the lower strength of this sample. Amount of dislocations were increased by the NC, thus the rapid increase in TTs was observed. On the other hand, S-CR5-SA550-1H-200MPa sample exhibited the longest fatigue life and the rate of the increase in TTs of this sample was observed to be less considering this long fatigue life.

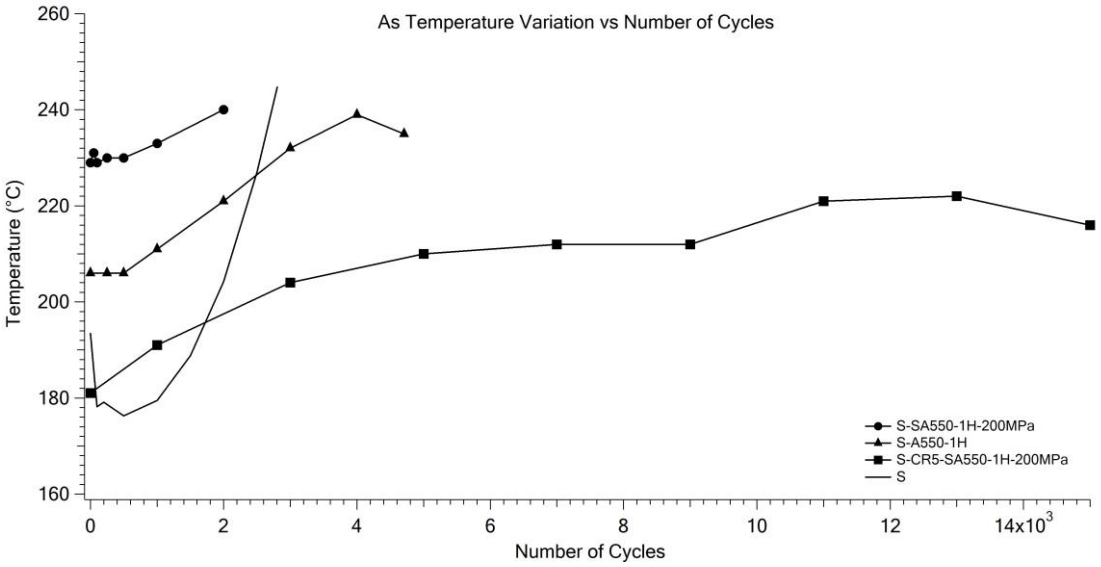

Figure 4.14. A_s Temperature Comparison of experimented samples with the cycle number

S-A550-1H and S-CR-SA550-1H-200MPa shows similar Af temperatures

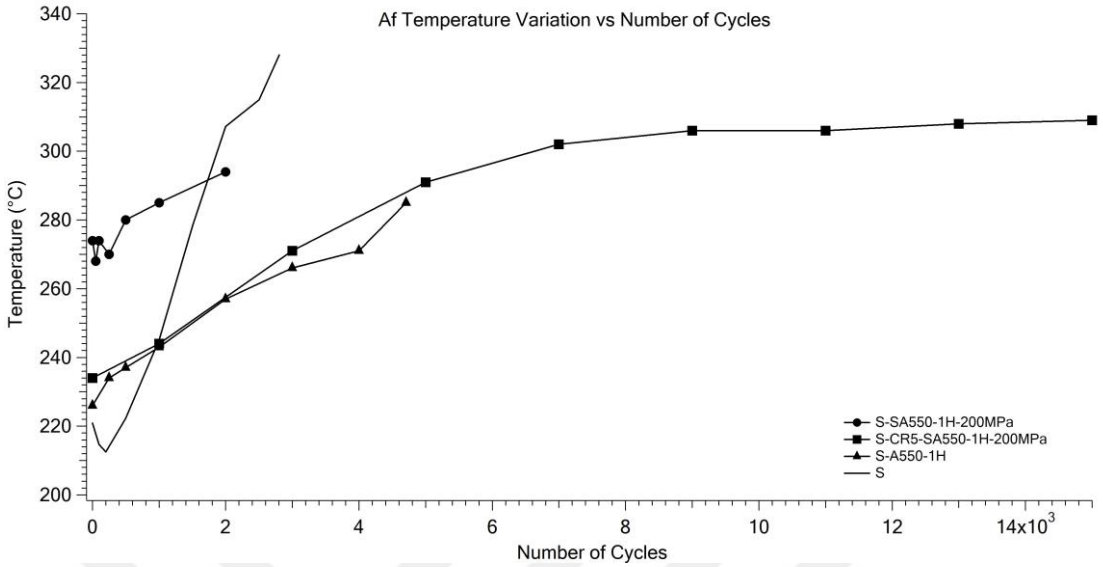

Figure 4.15. A_f Temperature Comparison of experimented samples with the cycle number

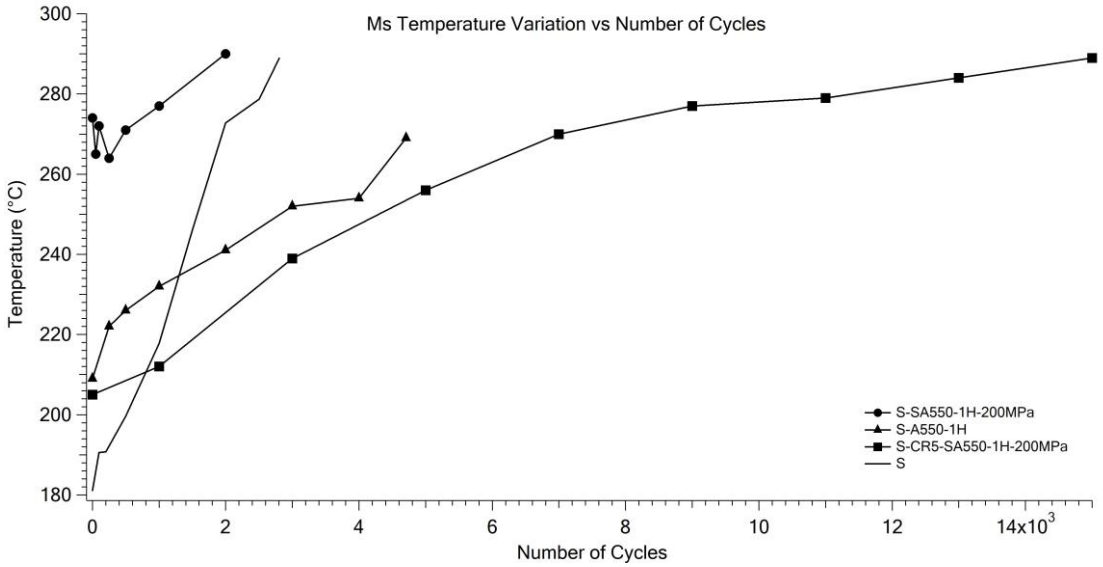

Figure 4.16. M_s Temperature Comparison of experimented samples with the cycle number

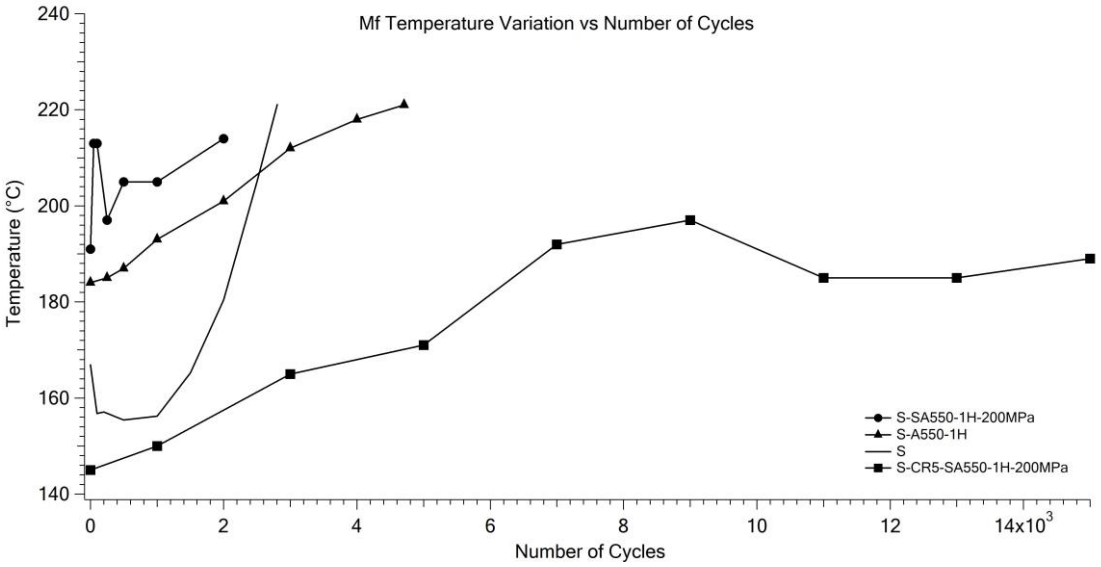

Figure 4.17. M_f Temperature Comparison of experimented samples with the cycle number

4.3.2. Austenite and Actuation Strain Comparisons

Two important strain magnitudes, which are ε_{aus} and ε_{act} are compared in this section since ε_{aus} provides the information of AIS by the NC and ε_{act} provides the information of transforming volume with the NC. Figure 4.18. and Figure 4.19. demonstrate the ε_{aus} and ε_{act} comparisons of all samples respectively.

There are a couple of important findings, which can be drawn from strain comparisons.

1) The AIS values of the S-CR5-SA550-1H-200MPa were increased to 0.2% during first 100 cycles and then the rate of increase in AIS was very small through the rest of the FFE. It can be stated that the AIS almost stayed constant throughout the FFE. The rate of the increase in AIS was observed to be very high for the S and S-SA550-1H-200MPa samples.

   It has been already known from the literature that strain hardening via applying deformation processes and age hardening with the formation of NP are the most important techniques to improve the cyclic stability of SMAs. As the SMAs get stronger, there is less dislocation storage during the heating-cooling cycles in FFE, so the shape memory properties stay constant. S-CR5-SA550-1H-200MPa sample was strengthened noticeably with the combined effect of cold rolling and stress

aging at 550C under 200MPa. Therefore, it was quite normal to observe the AIS stability in S-CR5-SA550-1H-200MPa sample.

2) ε_{act} values of all samples decreased with the NC but the rate of decrease in the S-CR5-SA550-1H-200MPa sample was the lowest. It can be stated that the ε_{act} of this sample almost stayed constant. However, it is also important to state that the ε_{act} values of S-CR5-SA550-1H-200MPa sample were determined to be the lowest throughout the FFE due to the NP, which cannot be transformed, and due to the increased number rolling induced dislocations. As the transforming volume of the S-CR5-SA550-1H-200MPa sample decreased the ε_{act} values were observed as the lowest one among all the other samples. NP formations were previously shown one of our research group's publications, which were demonstrated in Figure 2.4. However, it should be mentioned that the NPs, which were presented in this Figure, were randomly oriented precipitates since they were formed via aging without applying stress.
3) An intriguing finding is the observation of the highest ε_{aus} and ε_{act} values in FFE of S-SA550-1H since it was expected to determine the opposite of this observation. However, this might be due to the fact that, solutionized sample was directly stress aged at relatively high temperature under 200MPa and the stress application through tensile direction might lead to a formation of NP through unfavourable direction. The stress field around the unfavourably oriented NP may be the reason of gathering higher ε_{act}. If higher volume of transformation occurs there may be higher amount of dislocation storage with the transformation cycles. Therefore, higher accumulated strain values were attained from FFE of S-SA550-1H-200MPa sample.

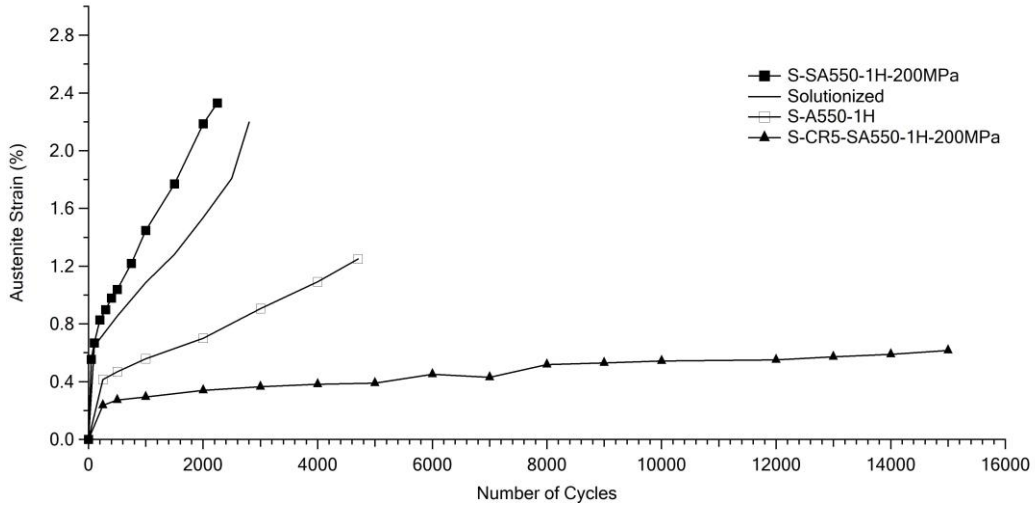

Figure 4.18. ε_{aus} comparison of all cycles.

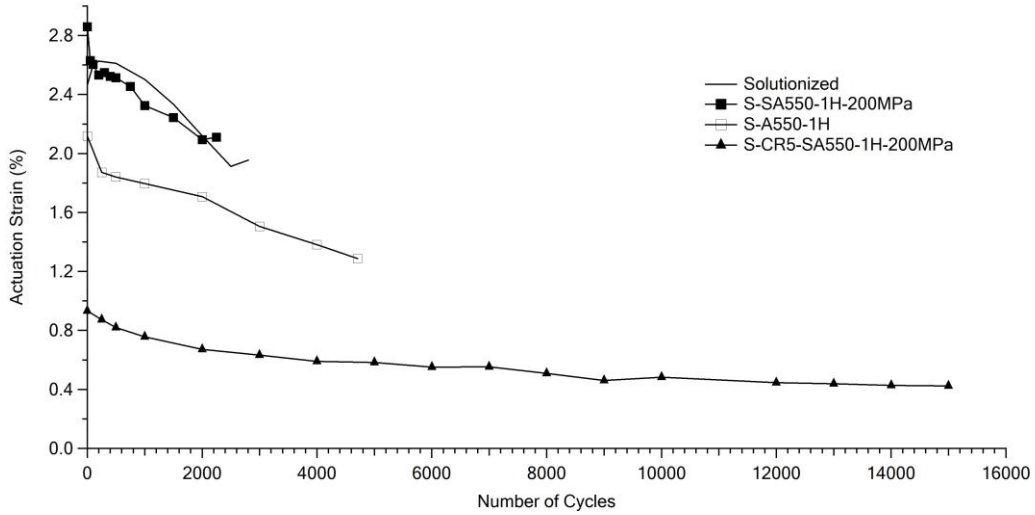

Figure 4.19. ε_{act} comparison of all samples

CONCLUSION

To clarify the effect of aging, stress assisted aging and cold rolling with successive stress assisted aging processes on functional fatigue and the SME properties of Ni(50.3at%)Ti(30at%)Hf(20at%) alloy, TT measurements and FFE experiments were conducted after applying the previously told thermal and thermo-mechanical processes. Regarding the experiment results shown in the preceding section, the following conclusions can be extracted in this study.

1) It was found from the DSC results that TTs increased as a result of aging for 1 hour at 550°C, whether the aging process was performed under stress or not. Aging under stress had quite a small effect on the change of TTs since almost no difference was observed between the TTs of S-A550-1H and S-SA550-1H-200MPa samples. Formation of NP with the aging heat treatment led to a drop in the Ni-amount of the matrix, therefore the TTs increased [4, 20].
2) The sample, which was CR and the stress aged at 550°C under 200MPa for 1 hr, also showed approximately same M_s, A_s and A_f temperatures with S-SA550-1H-200MPa. One can observe only a significant decrease in the M_f temperature of S-CR5-SA550-1H-200MPa sample with respect to other aged samples. Martensitic transformation was completed in this sample in a wide temperature range so the difference between M_s and M_f was determined as so large. This might be attributed to the increased dislocation concentration with the cold rolling process. These dislocations hinder the martensite boundary movement in the austenite phase by pinning the martensite-austenite phase boundaries.
3) FFEs were run under 200MPa on all samples between approximately 50°C-350°C. It was determined that TTs of S-A550-1H, S-SA550-1H-200MPa and S-CR5-SA550-1H-200MPa samples demonstrated an increasing tendency under the applied stress magnitude in FFEs. Shifting of TTs to higher values is an expected phenomenon since dislocation storage with the NC leads to pinning of mobile martensite-austenite phase boundaries and higher heat input is necessary to overcome the pinning effect such that the martensite-austenite transformation can continue.
4) ε_{act} values of all samples decreased by the NC but the rate of decline in the S-CR5-SA550-1H-200MPa sample was the lowest. It can be stated that the ε_{act} values of

this sample almost stayed constant but were determined to be the lowest throughout the FFE due to the NP, which cannot be transformed, and due to the increased number of rolling induced dislocations. As the transforming volume of the S-CR5-SA550-1 H-200MPa sample decreased, the ε_{act} values were observed as the lowest one but the fatigue life was determined to be the highest among all the other samples.

5) S-SA550-1H-200MPa sample presented the highest ε_{act} due to the stress fields around the oriented NP. The stress fields may lead an increase in transforming volume, so the ε_{act} increases. However, the increase in ε_{act} was obtained at the expense of fatigue life since S-SA-550-1H-200MPa sample was failed even earlier than that of the Solutionized sample.
6) Transmission Electron Microscopy studies should be done on all aged, stress aged and CR and stress aged samples to reveal especially the oriented NP formations via aging under stress. However, it is worth to mention that cold rolling with successive stress aging treatment led to a tremendous increase in the functional fatigue life of Ni-rich Ni(50.3at%)Ti(30at%)Hf(20at%) alloy with the increase in the stability of the ε_{act} at the expense of the decrease in the values.

REFERENCES

[1] Kockar, B., et al., *Thermomechanical cyclic response of an ultrafine-grained NiTi shape memory alloy.* Acta Materialia, 2008. **56**(14): p. 3630-3646.

[2] Ma, J., I. Karaman, and R.D. Noebe, *High temperature shape memory alloys.* International Materials Reviews, 2013. **55**(5): p. 257-315.

[3] Evirgen, A., et al., *Effect of precipitation on the microstructure and the shape memory response of the Ni50.3Ti29.7Zr20 high temperature shape memory alloy.* Scripta Materialia, 2013. **69**(5): p. 354-357.

[4] Tugrul, H.O., et al., *Comparison of the transformation behavior of cold rolling with aging and hot extrusion with aging processed Ni50.3Ti29.7Hf20 high temperature shape memory alloy.* Smart Materials and Structures, 2019. **28**(10).

[5] Yang, D., *Shape memory alloy and smart hybrid composites — advanced materials for the 21st Century.* Materials & Design, 2000. **21**(6): p. 503-505.

[6] Shayesteh Moghaddam, N., et al., *Achieving superelasticity in additively manufactured NiTi in compression without post-process heat treatment.* Sci Rep, 2019. **9**(1): p. 41.

[7] Otsuka, K. and X. Ren, *Recent developments in the research of shape memory alloys.* Intermetallics, 1999. **7**(5): p. 511-528.

[8] Duerig, T., D. Stoeckel, and D. Johnson, *SMA: smart materials for medical applications.* European Workshop on Smart Structures in Engineering and Technology. Vol. 4763. 2003: SPIE.

[9] Hartl, D.J. and D.C. Lagoudas, *Aerospace applications of shape memory alloys.* Proceedings of the Institution of Mechanical Engineers, Part G: Journal of Aerospace Engineering, 2007. **221**(4): p. 535-552.

[10] Reynolds, J.E. and M.B. Bever, *On the Reversal of the Strain-Induced Martensitic Transformation in the Copper-Zinc System.* JOM, 1952. **4**(10): p. 1065-1066.

[11] Dasgupta, R., *A look into Cu-based shape memory alloys: Present scenario and future prospects.* Journal of Materials Research, 2014. **29**(16): p. 1681-1698.

[12] Mazzer, E.M., M.R. da Silva, and P. Gargarella, *Revisiting Cu-based shape memory alloys: Recent developments and new perspectives.* Journal of Materials Research, 2022. **37**(1): p. 162-182.

[13] Cladera, A., et al., *Iron-based shape memory alloys for civil engineering structures: An overview.* Construction and Building Materials, 2014. **63**: p. 281-293.

[14] Abuzaid, W., et al., *FeMnNiAl Iron-Based Shape Memory Alloy: Promises and Challenges.* Shape Memory and Superelasticity, 2019. **5**(3): p. 263-277.

[15] T.MaruyamaH.Kubo, *Ferrous (Fe-based) shape memory alloys (SMAs): properties, processing and applications* Applications and Technologies Woodhead Publishing Series in Metals and Surface Engineering, 2011.

[16] Stoeckel, D., A. Pelton, and T. Duerig, *Self-expanding nitinol stents: material and design considerations.* Eur Radiol, 2004. **14**(2): p. 292-301.

[17] Hoh, D.J., et al., *Shape memory alloys: metallurgy, biocompatibility, and biomechanics for neurosurgical applications.* Neurosurgery, 2009. **64**(5 Suppl 2): p. 199-214; discussion 214-5.

[18] El Feninat, F., et al., *Shape Memory Materials for Biomedical Applications.* Advanced Engineering Materials, 2002. **4**(3): p. 91-104.

[19] Bigelow, G.S., et al., *Load-biased shape-memory and superelastic properties of a precipitation strengthened high-temperature Ni50.3Ti29.7Hf20 alloy.* Scripta Materialia, 2011. **64**(8): p. 725-728.

[20] Karaca, H.E., et al., *Effects of nanoprecipitation on the shape memory and material properties of an Ni-rich NiTiHf high temperature shape memory alloy.* Acta Materialia, 2013. **61**(19): p. 7422-7431.

[21] Khalil-Allafi, J., A. Dlouhy, and G. Eggeler, *Ni4Ti3-precipitation during aging of NiTi shape memory alloys and its influence on martensitic phase transformations.* Acta Materialia, 2002. **50**(17): p. 4255-4274.

[22] Radi, A., et al., *Influence of stress aging process on variants of nano-Ni4Ti3 precipitates and martensitic transformation temperatures in NiTi shape memory alloy.* Materials & Design, 2018. **142**: p. 93-100.

[23] Miyazaki, S., T. Kawai, and K. Otsuka, *STUDY OF FRACTURE IN Cu-Al-Ni SHAPE MEMORY BICRYSTALS.* Le Journal de Physique Colloques, 1982. **43**(C4): p. C4-813-C4-818.

[24] Kockar, B., et al., *Role of severe plastic deformation on the cyclic reversibility of a Ti50.3Ni33.7Pd16 high temperature shape memory alloy.* Acta Materialia, 2010. **58**(19): p. 6411-6420.

[25] Karaca, H.E., et al., *NiTiHf-based shape memory alloys.* Materials Science and Technology, 2014. **30**(13): p. 1530-1544.

[26] Demblon, A., et al., *Compositional and microstructural sensitivity of the actuation fatigue response in NiTiHf high temperature shape memory alloys.* Materials Science and Engineering: A, 2022. **838**.

[27] Prokoshkin, S., et al., *Formation of nanostructures in thermomechanically-treated Ti–Ni and Ti–Nb-(Zr, Ta) SMAs and their roles in martensite crystal lattice changes and mechanical behavior.* Journal of Alloys and Compounds, 2013. **577**: p. S418-S422.

[28] Kockar, B., et al., *A method to enhance cyclic reversibility of NiTiHf high temperature shape memory alloys.* Scripta Materialia, 2006. **54**(12): p. 2203-2208.

[29] Evirgen, A., et al., *EFFECT OF AGING ON THE MARTENSITIC TRANSFORMATION CHARACTERISTICS OF A Ni-RICH NiTiHf HIGH TEMPERATURE SHAPE MEMORY ALLOY.* Functional Materials Letters, 2012. **05**(04): p. 1250038.

[30] Evirgen, A., et al., *Microstructural characterization and shape memory characteristics of the Ni50.3Ti34.7Hf15 shape memory alloy.* Acta Materialia, 2015. **83**: p. 48-60.

[31] Saghaian, S.M., et al., *Tensile shape memory behavior of Ni50.3Ti29.7Hf20 high temperature shape memory alloys.* Materials & Design, 2016. **101**: p. 340-345.

[32] Karakoc, O., et al., *Effects of upper cycle temperature on the actuation fatigue response of NiTiHf high temperature shape memory alloys.* Acta Materialia, 2017. **138**: p. 185-197.

[33] Abuzaid, W. and H. Sehitoglu, *Functional fatigue of Ni50.3Ti25Hf24.7 – Heterogeneities and evolution of local transformation strains.* Materials Science and Engineering: A, 2017. **696**: p. 482-492.

[34] Sehitoglu, H., Y. Wu, and L. Patriarca, *Shape memory functionality under multi-cycles in NiTiHf.* Scripta Materialia, 2017. **129**: p. 11-15.

[35] Saygili, H.H., H.O. Tugrul, and B. Kockar, *Effect of Aging Heat Treatment on the High Cycle Fatigue Life of Ni50.3Ti29.7Hf20 High-Temperature Shape Memory Alloy.* Shape Memory and Superelasticity, 2018. **5**(1): p. 32-41.

[36] Potapov, P.L., et al., *Effect of Hf on the structure of Ni-Ti martensitic alloys.* Materials Letters, 1997. **32**(4): p. 247-250.

[37] Prasher, M., et al., *Effect of Hf solute addition on the phase transformation behavior and hardness of a Ni-rich NiTi alloy.* Materials Chemistry and Physics, 2020. **247**.

[38] Besseghini, S., E. Villa, and A. Tuissi, *Ni・Ti・Hf shape memory alloy: effect of aging and thermal cycling.* Materials Science and Engineering: A, 1999. **273-275**: p. 390-394.

[39] Meng, X.L., et al., *Effect of aging on martensitic transformation and microstructure in Ni-rich TiNiHf shape memory alloy.* Scripta Materialia, 2006. **54**(9): p. 1599-1604.

[40] Saghaian, S.M., et al., *Effects of aging on the shape memory behavior of Ni-rich Ni50. 3Ti29. 7Hf20 single crystals.* Acta Materialia, 2015. **87**: p. 128-141.

[41] Babacan, N., et al., *Effects of cold and warm rolling on the shape memory response of Ni50Ti30Hf20 high-temperature shape memory alloy.* Acta Materialia, 2018. **157**: p. 228-244.

[42] Treppmann, D. and E. Hornbogen, *On the Influence of Thermomechanical Treatments on Shape Memory Alloys.* Le Journal de Physique IV, 1997. **07**(C5): p. C5-211-C5-220.

[43] Frick, C.P., et al., *Thermal processing of polycrystalline NiTi shape memory alloys.* Materials Science and Engineering: A, 2005. **405**(1-2): p. 34-49.

[44] Gall, K., et al., *Effect of microstructure on the fatigue of hot-rolled and cold-drawn NiTi shape memory alloys.* Materials Science and Engineering: A, 2008. **486**(1-2): p. 389-403.

[45] Acar, E., et al., *On the stress-assisted aging in NiTiHfPd single crystal shape memory alloys.* Materials Science and Engineering: A, 2018. **725**: p. 51-56.

[46] Velipaşaoğlu, M.S., *The Determination of The Functional Fatigue Life of High Temperature Shape Memory Alloys After Cold Rolling Process.* 2020.